

Figure 1

60x43mm (300 x 300 DPI)

1
2
3
4
5
6
7
8
9
10
11
12
13
14
15
16
17
18
19
20
21
22
23
24
25
26
27
28
29
30
31
32
33
34
35
36
37
38
39
40
41
42
43
44
45
46
47
48
49
50
51
52
53
54
55
56
57
58
59
60

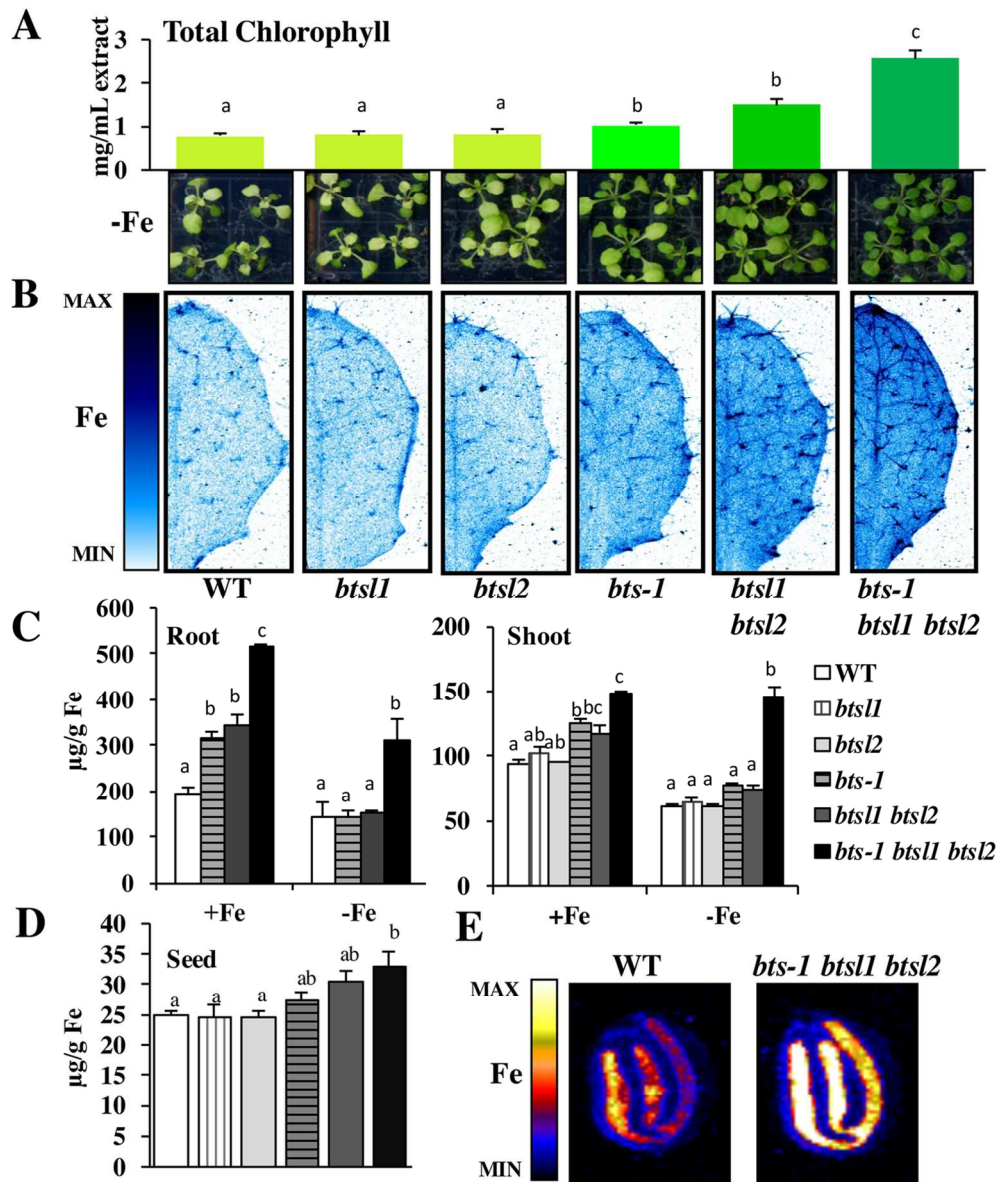


Figure 2

119x142mm (300 x 300 DPI)

1
2
3
4
5
6
7
8
9
10
11
12
13
14
15
16
17
18
19
20
21
22
23
24
25
26
27
28
29
30
31
32
33
34
35
36
37
38
39
40
41
42
43
44
45
46
47
48
49
50
51
52
53
54
55
56
57
58
59
60

1
2
3
4
5
6
7
8
9
10
11
12
13
14
15
16
17
18
19
20
21
22
23
24
25
26
27
28
29
30
31
32
33
34
35
36
37
38
39
40
41
42
43
44
45
46
47
48
49
50
51
52
53
54
55
56
57
58
59
60

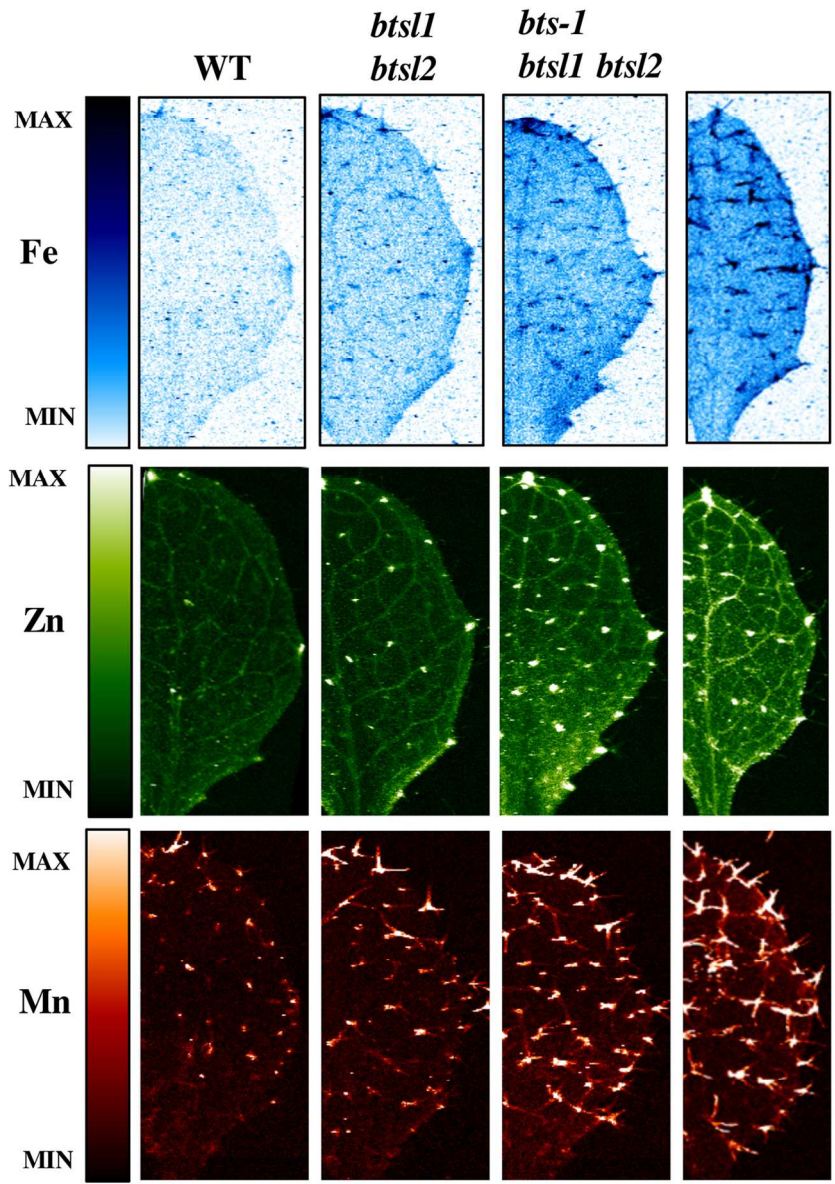


Figure 3

117x165mm (300 x 300 DPI)

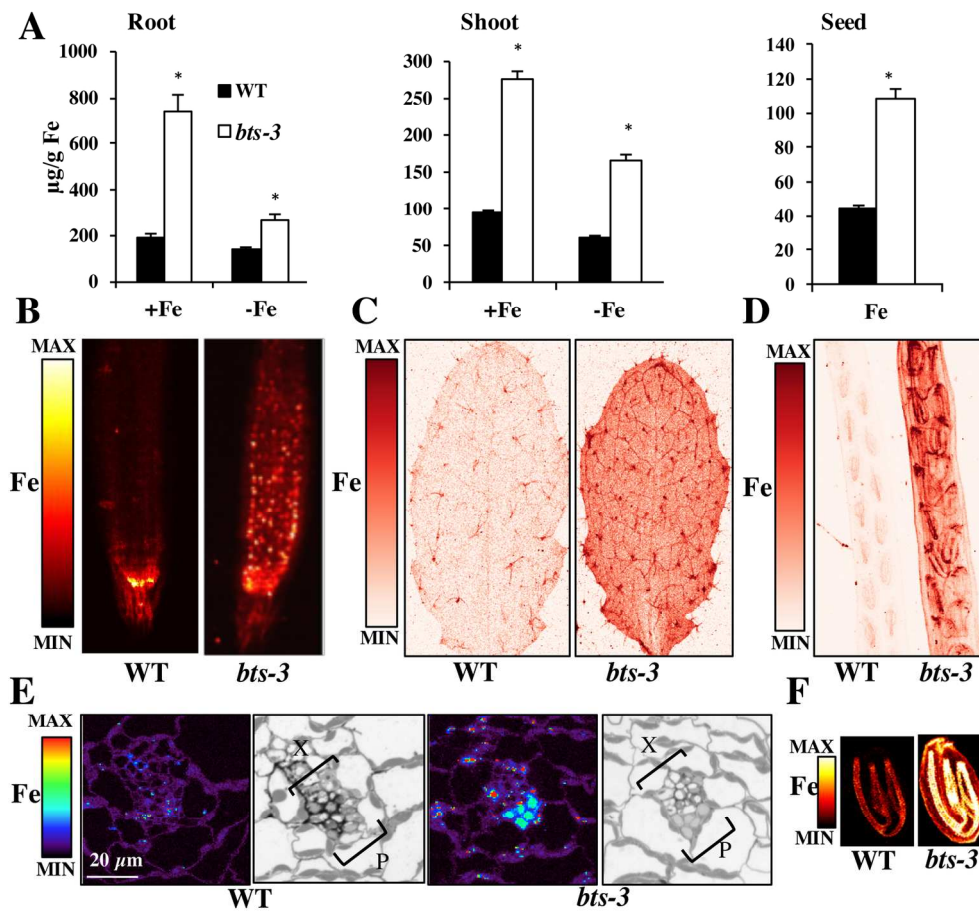


Figure 4

156x142mm (300 x 300 DPI)

1
2
3
4
5
6
7
8
9
10
11
12
13
14
15
16
17
18
19
20
21
22
23
24
25
26
27
28
29
30
31
32
33
34
35
36
37
38
39
40
41
42
43
44
45
46
47
48
49
50
51
52
53
54
55
56
57
58
59
60

1
2
3
4
5
6
7
8
9
10
11
12
13
14
15
16
17
18
19
20
21
22
23
24
25
26
27
28
29
30
31
32
33
34
35
36
37
38
39
40
41
42
43
44
45
46
47
48
49
50
51
52
53
54
55
56
57
58
59
60

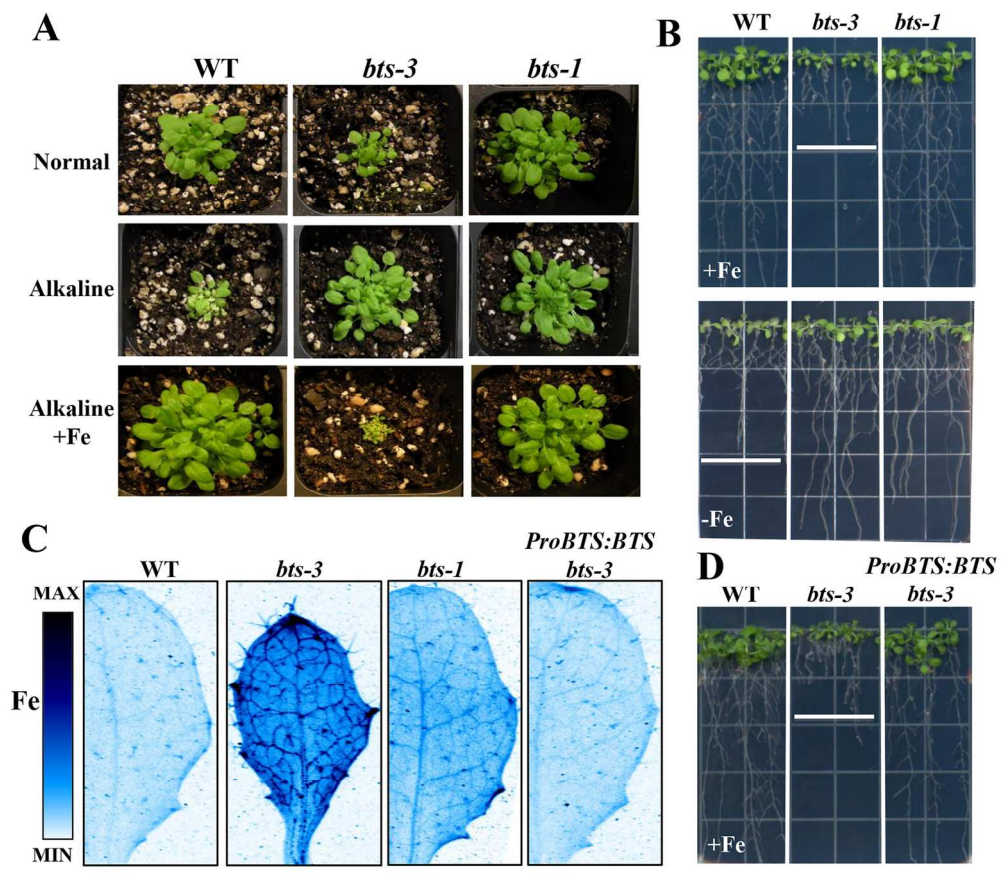


Figure 5

148x128mm (300 x 300 DPI)

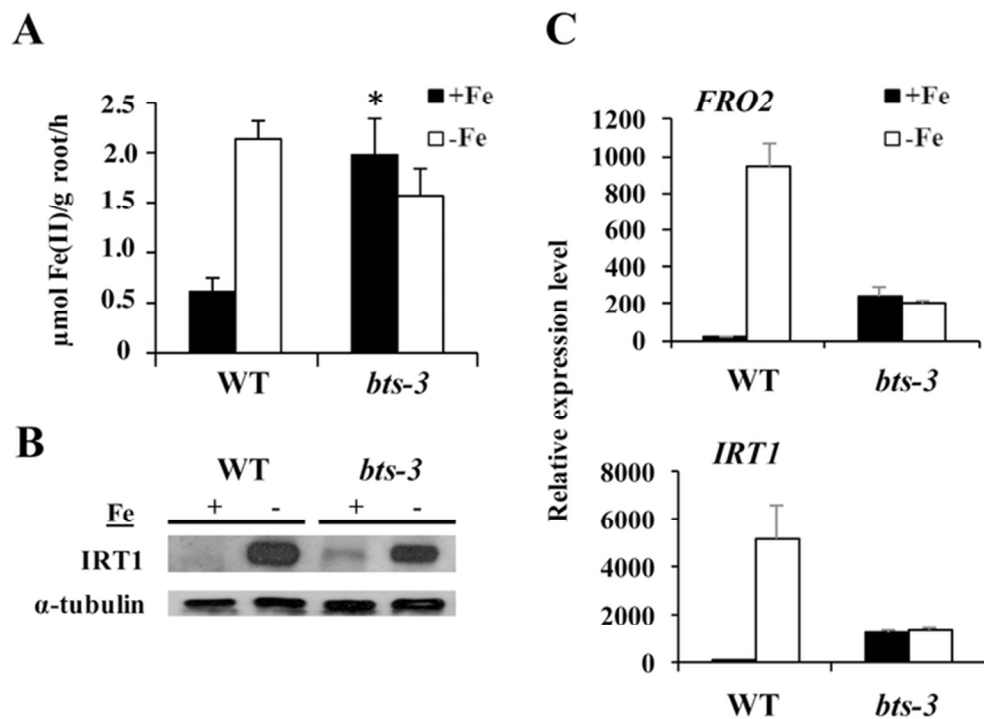


Figure 6

60x44mm (300 x 300 DPI)

1
2
3
4
5
6
7
8
9
10
11
12
13
14
15
16
17
18
19
20
21
22
23
24
25
26
27
28
29
30
31
32
33
34
35
36
37
38
39
40
41
42
43
44
45
46
47
48
49
50
51
52
53
54
55
56
57
58
59
60

1
2
3
4
5
6
7
8
9
10
11
12
13
14
15
16
17
18
19
20
21
22
23
24
25
26
27
28
29
30
31
32
33
34
35
36
37
38
39
40
41
42
43
44
45
46
47
48
49
50
51
52
53
54
55
56
57
58
59
60

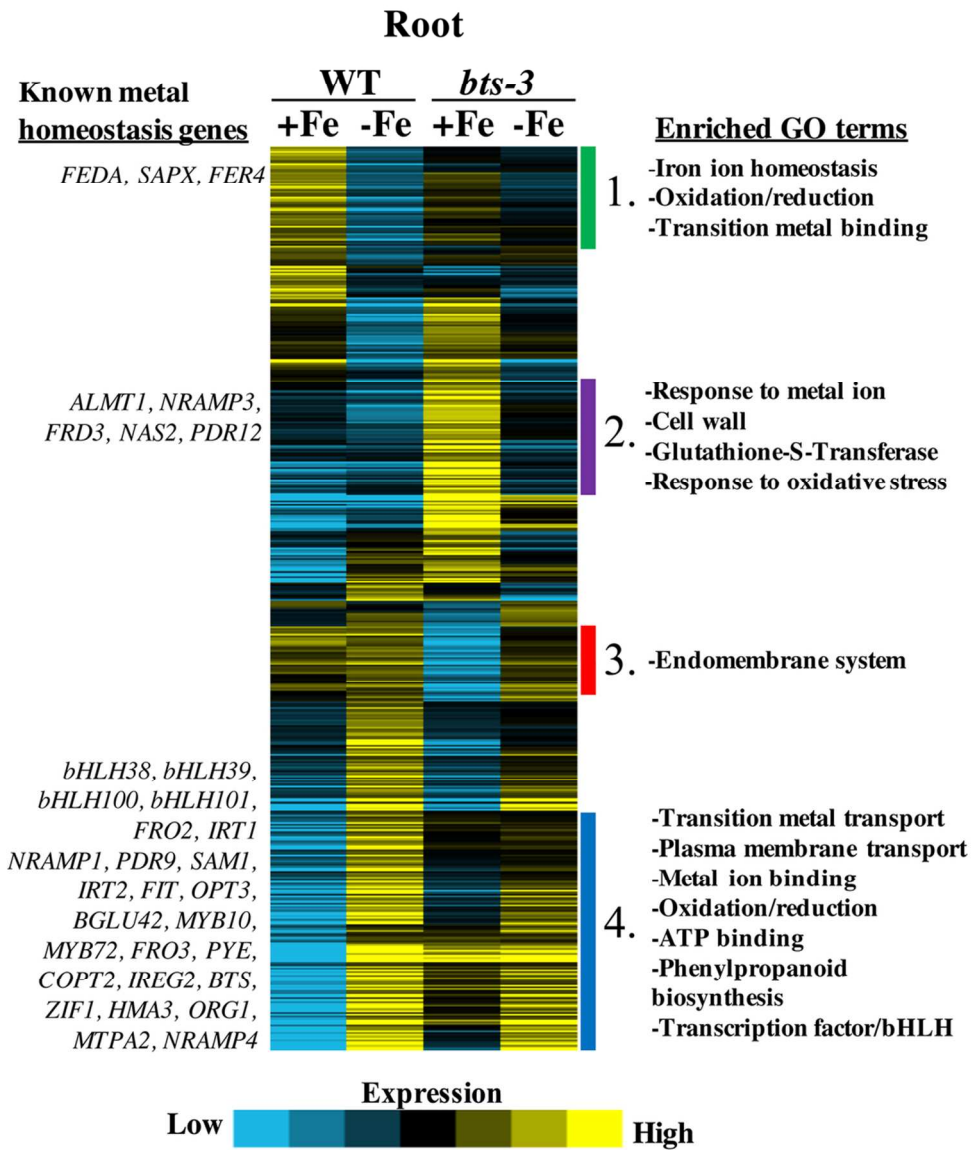


Figure 7

98x118mm (300 x 300 DPI)

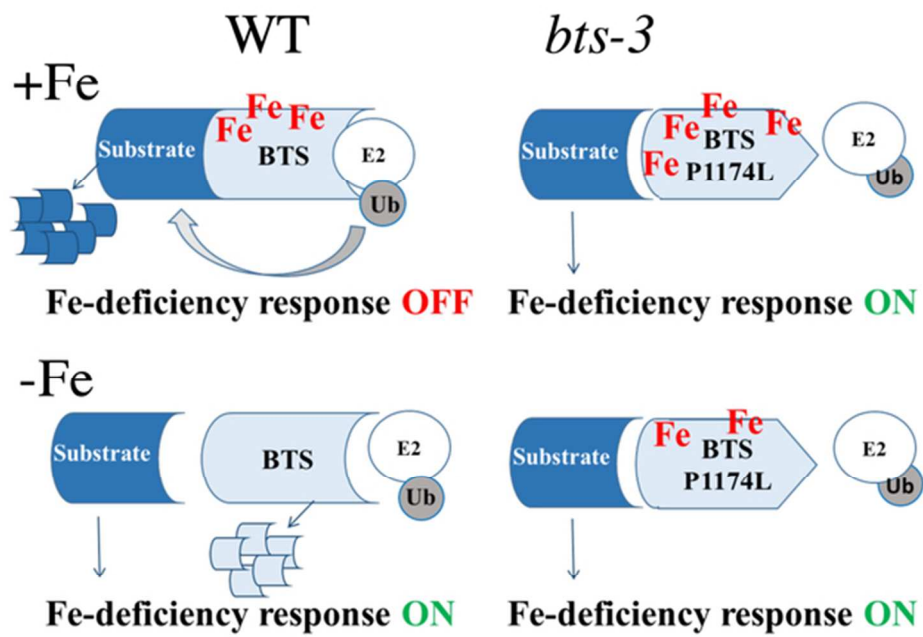
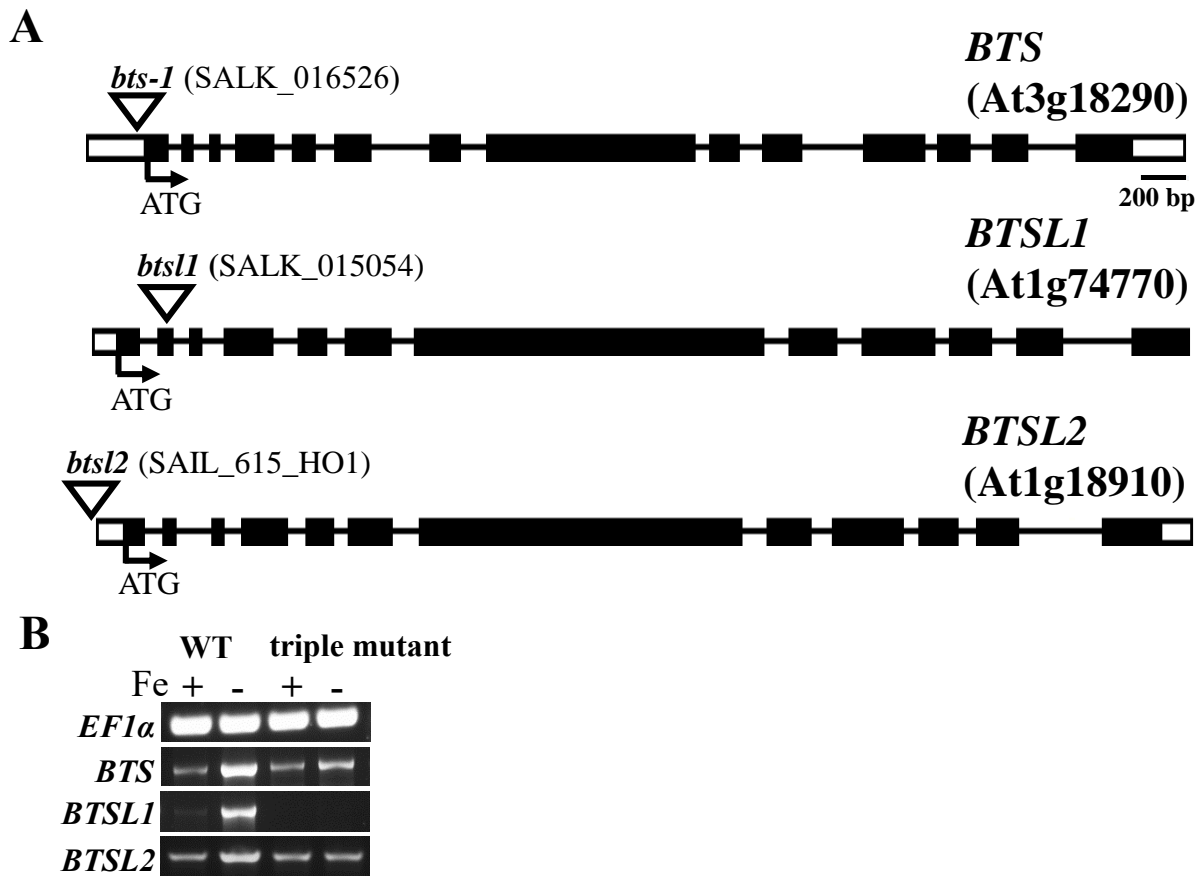


Figure 8

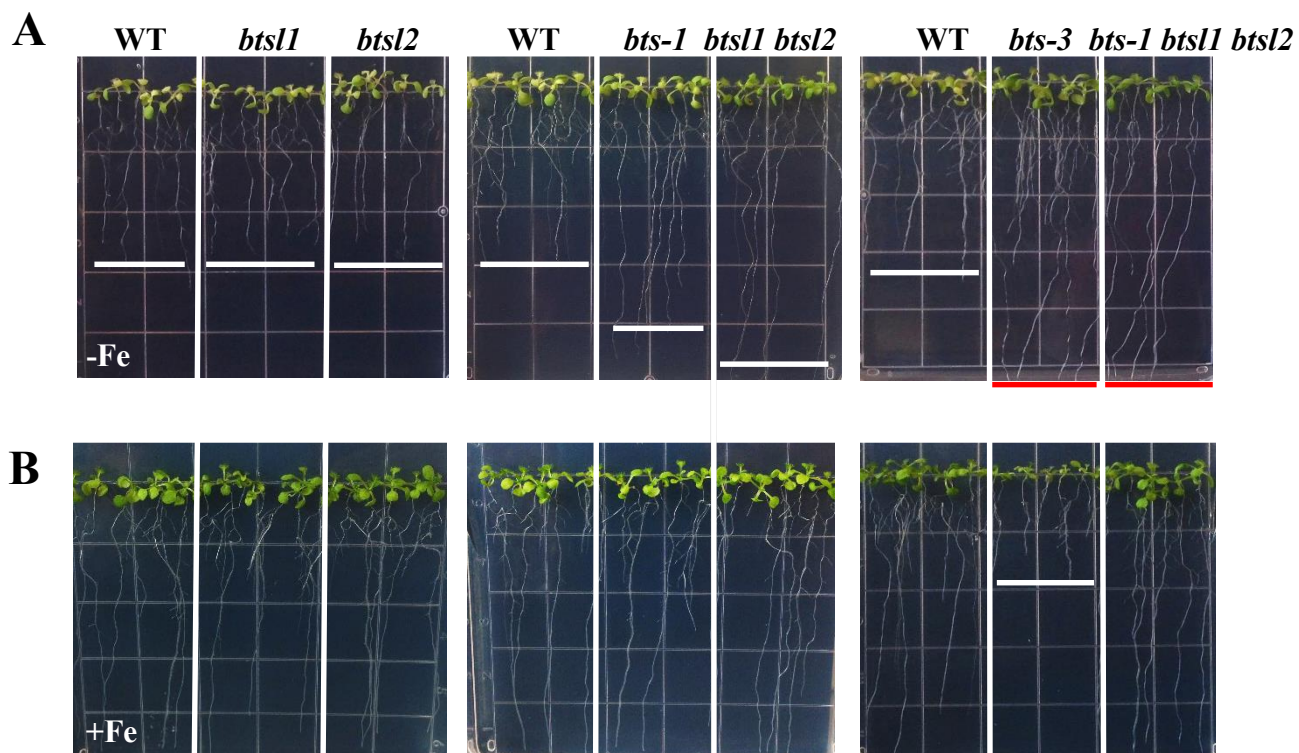
57x39mm (300 x 300 DPI)

1
2
3
4
5
6
7
8
9
10
11
12
13
14
15
16
17
18
19
20
21
22
23
24
25
26
27
28
29
30
31
32
33
34
35
36
37
38
39
40
41
42
43
44
45
46
47
48
49
50
51
52
53
54
55
56
57
58
59
60



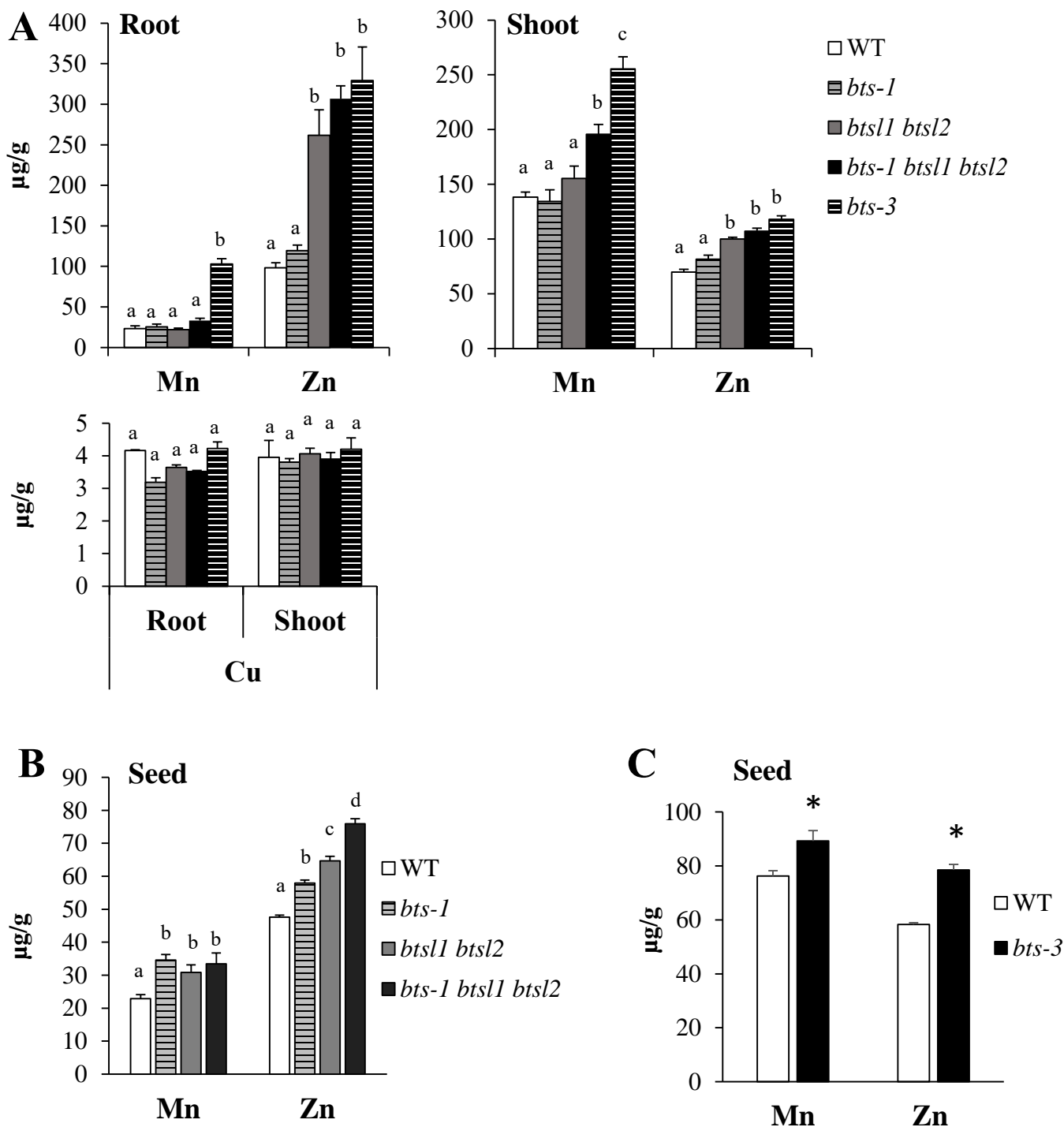
Supplemental Figure 1. Location of T-DNA insertions of *bts-1*, *bts11* and *bts12* mutants.

A. Arrows indicate position of T-DNA insertions within *BTS*, *BTSL1*, and *BTSL2* genes. Black boxes represent exons, lines indicate introns, and white boxes indicate UTRs. The *bts-1* insertion occurs in the 5'UTR, the insertion in *bts11* occurs in the 2nd exon, and the insertion in *bts12* occurs in the promoter just before the 5'UTR. **B.** Full length transcript amplified from cDNA of roots of plants grown for 2 weeks on B5 medium and then transferred to +Fe or -Fe medium for 3 days.



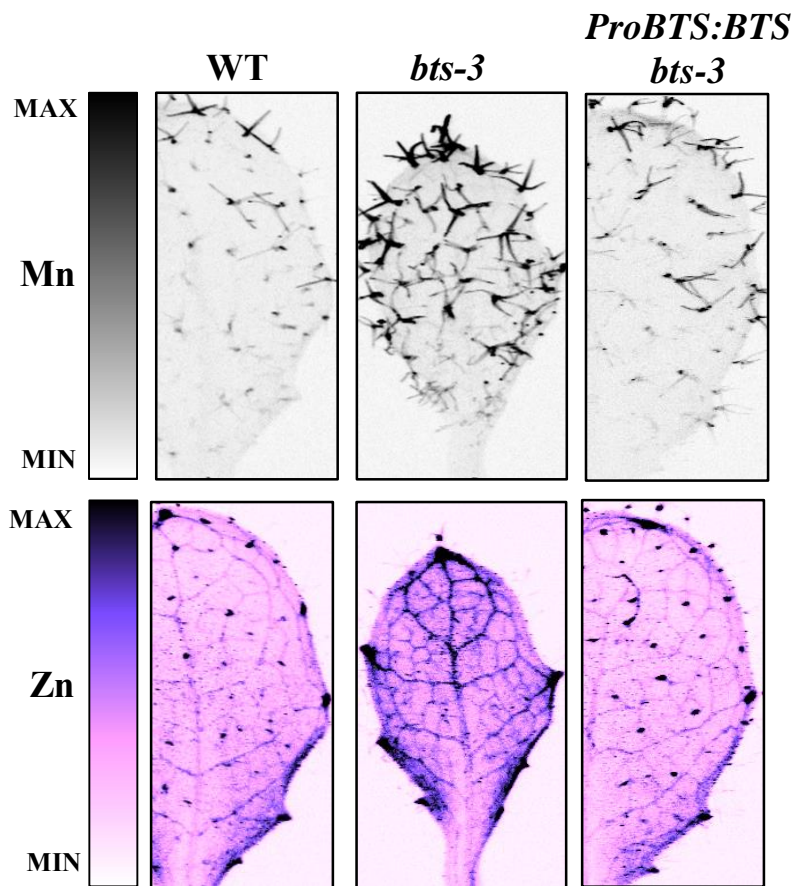
Supplemental Figure 2. *bts-1*, *bts11* *bts12*, *bts-1* *bts11* *bts12*, and *bts-3* mutants all exhibit tolerance to Fe-deficient growth conditions, but only *bts-3* is sensitive to Fe-sufficient conditions.

Plants were grown vertically for 5 days on B5 medium and then transferred to +Fe (A) or -Fe medium (B) for 7 days.



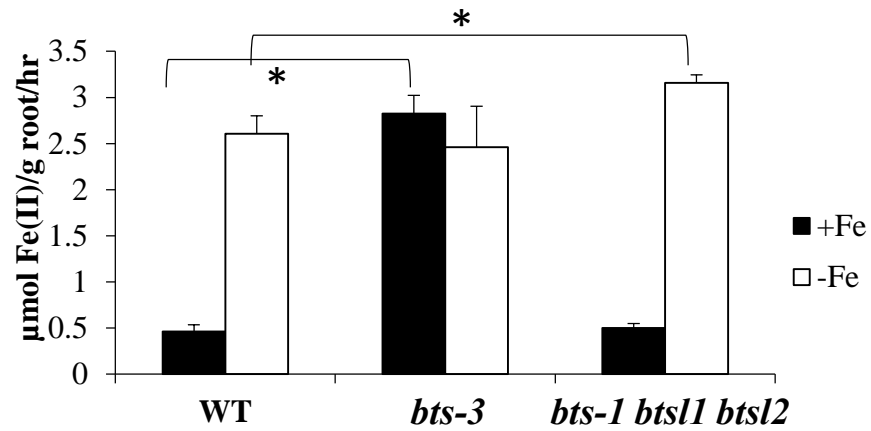
Supplemental Figure 3. BTS family E3 ligase mutants have higher Mn and Zn concentrations in roots, shoots and seeds compared to wild type.

A. Root and shoot ICP-MS measurements of plants grown for 2 weeks on B5 and then transferred to +Fe medium for 3 days. **B.** Seed ICP-MS measurements of harvest from soil grown plants (as in Figure 2). Lower case letters indicate significant differences at $p < 0.05$ (ANOVA with Tukey's). **C.** Seed ICP-MS measurements of harvest from soil grown plants. * indicates $p < 0.05$ compared to WT (Student's T-test).



Supplemental Figure 4. Expression of *BTS* controlled by its endogenous promoter in *bts-3* returns Mn and Zn levels to wild type levels.

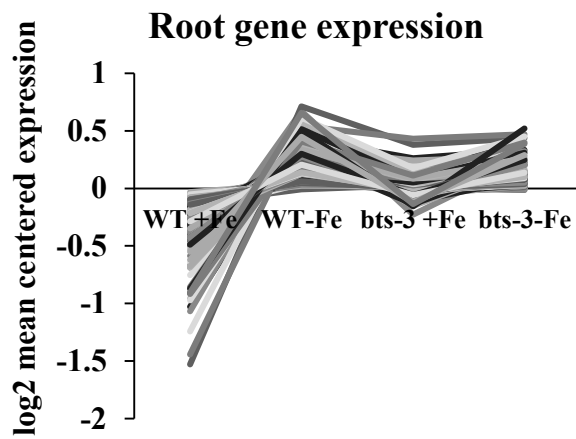
SXRF scans showing Fe localization in leaf #5 of plants grown for 2 weeks on B5 medium and then transferred to +Fe medium for 3 days. *ProBTS:BTS bts-3* is the complementation line where the *BTS* gene driven by its own promoter is expressed in the *bts-3* mutant.



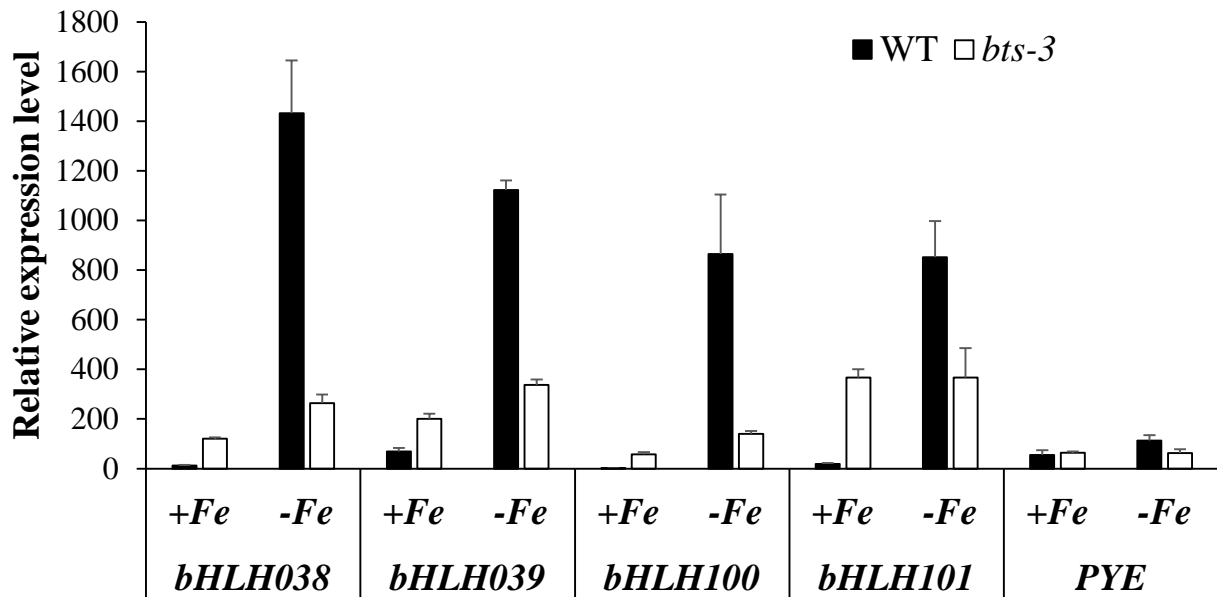
Supplemental Figure 5. Unlike *bts-3*, *bts-1 btsl1 btsl2* mutants do not exhibit induction of ferric chelate reductase activity when grown under Fe-sufficient conditions.

Ferric chelate reductase activity of roots of plants grown for 2 weeks on B5 medium before transfer to +Fe or -Fe medium for 3 days. * $p < 0.05$ (Student's t-test). Brackets indicate comparisons. Error bars indicate SE.

A



B



Supplemental Figure 6. *bts-3* roots exhibit constitutive expression of Fe deficiency genes.

A. Line graphs showing gene expression profiles of all genes from cluster 4 of root microarray analysis.

B. qPCR of bHLH transcription factor expression in roots of plants grown for 2 weeks on B5 medium and then transferred to +Fe or -Fe medium for 3 days. Expression is relative to EF1 α . Error bars represent SE (n=3).

1
2
3
4
5
6
7
8
9
10
11
12
13
14
15
16
17
18
19
20
21
22
23
24
25
26
27
28
29
30
31
32
33
34
35
36
37
38
39
40
41
42
43
44
45
46
47
48
49
50
51
52
53
54
55
56
57
58
59
60

Supplemental methods: SXRF analysis

Plants for NSLS leaf SXRF experiments were grown for 2 weeks on B5 and 3 days on +Fe or -Fe medium. Leaf #5 from plants of each genotype was detached and mounted on the sample stage on metal free KaptonTM tape just prior imaging. X26A and X27A use Kirkpatrick-Baez (KB) mirror microprobes and a Ge detector. Incident energy for each leaf image was 11 keV, step size was 10 μm and dwell time was 100 milliseconds. Dry seeds from soil-grown plants imaged at NSLS were also mounted on KaptonTM tape and scanned with a 5 μm step size and 100 millisecond dwell time.

Roots, leaves, and siliques for SSRL experiments were detached and mounted on KaptonTM tape from plants just prior to analysis. Roots were from that were grown for 7 days on B5 medium and 3 days on -Fe medium. Leaf #8 for shoot images was from plants grown for 10 days on B5 medium. Green, developed siliques were from plants grown on soil. Beamline 2-3 also uses a KB mirror microprobe with a Ge detector. Root images had a step size of 1 μm and dwell time of 100 milliseconds. Leaves had a 7 μm step size and 30 millisecond dwell time. Siliques had a 7 μm step size and 50 millisecond dwell time.

Dry seeds imaged at XFM were from soil grown plants and mounted on metal free Ultralene thin window film[®]. A KB mirror microprobe was used with the Maia detector, a Si detector (Ryan et al., 2010). Incident energy was 11 keV, step size was 2 μm and dwell time was 2.6 milliseconds.

High resolution imaging of leaf sections were conducted at 2-ID-D of the Advanced Photon Source. Plants were grown on B5 medium for 10 days and leaf #1 was fixed for sectioning. Sample preparation was performed as described, using LR White embedding resin, 1 μm thick sectioning, and mounting on silicon nitride windows (Punshon et al., 2012). The 2-ID-D beamline uses a zone plate insertion device to achieve a highly focused beam. Imaging was conducted using an incident energy of 10.1 keV, 0.15 μm step size, and 500 millisecond dwell time.

Data gathered at SSRL was analyzed with Sam's Microtool Analysis Kit (SMAK) (microtoolkit.sams-xrays.com), data from NSLS was processed with Xmap Plotter (bnl.gov/x26a/comp_download.shtml) and data from the Australian Synchrotron was analyzed with Image J (<http://imagej.nih.gov/ij/>). Images are false colored to show fluorescence counts detected on a scale from minimum to maximum for specific elements. Images that are directly compared are scaled to the same minimum and maximum fluorescence counts.

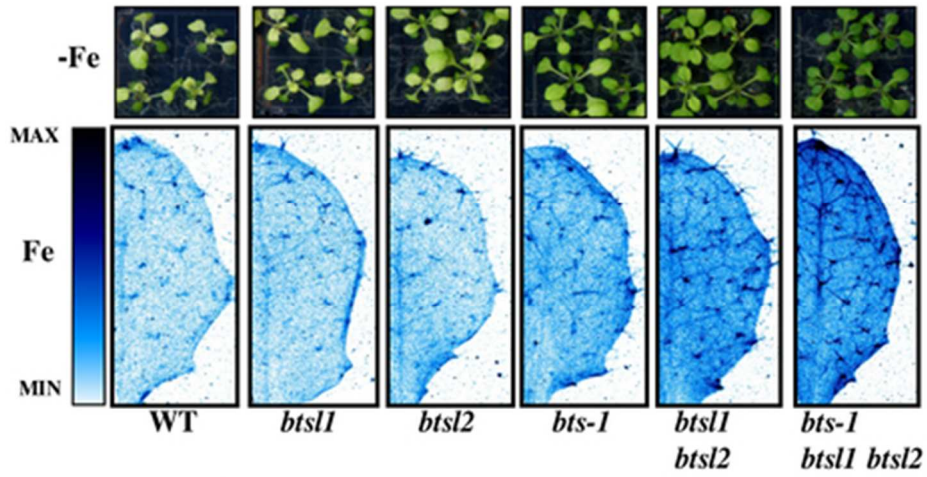
Supplemental References

Punshon, T., Hirschi, K., Yang, J., Lanzirotti, A., Lai, B., and Guerinot, M.L. (2012). The role of CAX1 and CAX3 in elemental distribution and abundance in Arabidopsis seed. *Plant Physiol.* **158**, 352-362.

Ryan, C.G., Kirkham, R., Hough, R.M., Moorhead, G., Siddons, D.P., de Jonge, M.D., Paterson, D.J., De Geronimo, G., Howard, D.L., and Cleverley, J.S. (2010). Elemental X-ray imaging using the Maia detector array: The benefits and challenges of large solid-angle. *Nucl. Instrum. Meth. A.* **619**, 37-43.

1
2
3
4
5
6
7
8
9
10
11
12
13
14
15
16
17
18
19
20
21
22
23
24
25
26
27
28
29
30
31
32
33
34
35
36
37
38
39
40
41
42
43
44
45
46
47
48
49
50
51
52
53
54
55
56
57
58
59
60

1
2
3
4
5
6
7
8
9
10
11
12
13
14
15
16
17
18
19
20
21
22
23
24
25
26
27
28
29
30
31
32
33
34
35
36
37
38
39
40
41
42
43
44
45
46
47
48
49
50
51
52
53
54
55
56
57
58
59
60



BTS family members negatively regulate the Fe deficiency response; mutants have increased Fe levels and tolerance to Fe deficiency.

39x30mm (300 x 300 DPI)

1
2
3
4
5 ***BRUTUS* and its paralogs, *BTS LIKE1* and *BTS LIKE2*, encode important negative**
6 **regulators of the iron deficiency response in *Arabidopsis thaliana***
7
8

9
10 **Running title: E3 ligases mediate *Arabidopsis* Fe homeostasis**
11

12
13
14 Maria N. Hindt^a, Garo Z. Akmakjian^a, Kara L. Pivarski^a, Tracy Punshon^a, Ivan Baxter^b, David E.
15 Salt^c, and Mary Lou Guerinot^{a1}
16
17

18
19
20
21 ^a Department of Biological Sciences, Dartmouth College, Hanover, NH, 03755

22 ^b USDA-ARS Plant Genetics Research Unit, Donald Danforth Plant Sciences Center, St. Louis
23 Missouri 63132, USA.
24

25
26 ^c Institute of Biological and Environmental Sciences, University of Aberdeen, Aberdeen,
27 Scotland AB24 3UU, United Kingdom
28
29

30
31 Current Address:

32
33 DES: School of Biosciences, University of Nottingham, Sutton Bonington Campus,
34 Loughborough, Leicestershire LE12 5RD, UK
35
36

37
38
39 ¹ Address correspondence to Guerinot@Dartmouth.edu.
40
41
42
43
44
45
46
47
48
49
50
51
52
53
54
55
56
57
58
59
60

Abstract

Iron (Fe) is required for plant health, but it can also be toxic when present in excess. Therefore, Fe levels must be tightly controlled. The *Arabidopsis thaliana* E3 ligase BRUTUS (BTS) is involved in the negative regulation of the Fe deficiency response and we show here that the two *A. thaliana* BTS paralogs, *BTS LIKE1* (*BTSL1*) and *BTS LIKE2* (*BTSL2*) encode proteins that act redundantly as negative regulators of the Fe deficiency response. Loss of both of these E3 ligases enhances tolerance to Fe deficiency. We further generated a triple mutant with loss of both *BTS* paralogs and a partial loss of *BTS* expression that exhibits even greater tolerance to Fe-deficient conditions and increased Fe accumulation without any resulting Fe toxicity effects. Finally, we identified a mutant carrying a novel missense mutation of *BTS* that exhibits an Fe deficiency response in the root when grown under both Fe-deficient and Fe-sufficient conditions, leading to Fe toxicity when plants are grown under Fe-sufficient conditions.

Significance to Metalloids

Iron (Fe) deficiency commonly limits plant growth. If Fe homeostasis were understood, it might be feasible to engineer plants better able to grow in soils now considered marginal and to increase crop biomass on soils now in cultivation. Furthermore, as most people rely on plants as their dietary source of Fe, plants that serve as better sources of this essential nutrient would improve human health. In this study, we characterize the role of three closely related negative regulators of the Fe deficiency response. A triple mutant has increased tolerance to Fe deficient growth conditions and increased Fe accumulation without resulting toxicity.

Introduction

Iron (Fe) is essential for plant growth, crop yields and human health. Many people, particularly those in developing countries, rely on plants for dietary Fe. Unfortunately, Fe has a limited solubility in many neutral or basic soils and therefore Fe is not readily accessible in the rhizosphere¹. This low solubility leads to a restricted Fe content in many plants and is a major factor contributing to the widespread prevalence of Fe deficiency anemia for people with plant-based diets. Thus, increasing plant Fe acquisition and storage may have profound impacts on plant and human nutrition. In order to manipulate plants to increase bioavailable Fe, it is first imperative we understand the genes and mechanisms governing Fe homeostasis in plants. When

1
2
3
4
5
6
7
8
9
10
11
12
13
14
15
16
17
18
19
20
21
22
23
24
25
26
27
28
29
30
31
32
33
34
35
36
37
38
39
40
41
42
43
44
45
46
47
48
49
50
51
52
53
54
55
56
57
58
59
60

faced with low Fe conditions, non-graminaceous plants such as *Arabidopsis thaliana* (*Arabidopsis*) employ a classic response to boost Fe mobilization and uptake from the soil. Root plasma membrane H⁺-ATPases release protons to acidify and thus increase Fe solubility in the soil². In addition to acidification, Fe³⁺ is reduced to Fe²⁺ by the membrane-bound ferric-chelate reductase enzyme FERRIC OXIDASE REDUCTASE 2 (*FRO2*) in *Arabidopsis*³. Fe deficiency also induces root secretion of phenolic compounds, particularly coumarins, which serve as direct Fe³⁺ reductants and also as Fe³⁺ and Fe²⁺ chelating compounds to improve Fe mobilization and reduction⁴⁻⁷. This series of mechanisms is known as the reduction strategy or alternatively Strategy I¹. Reduced Fe is transported into the root by the plasma-membrane divalent cation transporter IRON-REGULATED TRANSPORTER 1 (*IRT1*)⁸⁻¹¹.

These activities to boost Fe mobilization under Fe-deficient conditions are controlled by several transcription factors in *Arabidopsis*. One major transcription factor identified in a well-characterized Fe deficiency network is a bHLH protein called FER-LIKE IRON DEFICIENCY-INDUCED TRANSCRIPTION FACTOR (*FIT*)¹²⁻¹⁴. Like *IRT1* and *FRO2*, *FIT* is induced in the root epidermis in Fe deficiency and expression of *IRT1* and *FRO2* requires *FIT*¹²⁻¹⁴. Other bHLH transcription factors which are induced in Fe-deficient conditions are those of the bHLH1b subfamily (bHLH38, bHLH39, bHLH100, bHLH101) and evidence suggests that *FIT* activity and activation of downstream Fe deficiency targets depends on heterodimerization of *FIT* with one of these bHLH transcription factors¹⁴⁻¹⁷. *FIT* also controls *MYB10* and *MYB72*, two other transcription factors essential for growth of plants on low Fe conditions^{12, 18, 19}.

Another set of transcriptional changes upon Fe deficiency occurs in the vasculature. A major player identified in this network is another bHLH transcription factor called POPEYE (*PYE*)²⁰. *PYE* expression is highest in the root pericycle, but *PYE* protein is localized to the nuclei of all cells in Fe-deficient roots, suggesting that *PYE* may move throughout the root, linking it to the *FIT* network. *PYE* has been shown to negatively regulate the expression of known Fe deficiency targets *NICOTIANAMINE SYNTHASE 4* (*NAS4*), *FERRIC REDUCTASE OXIDASE 3* (*FRO3*), and *ZINC-INDUCED FACILITATOR* (*ZIF1*). Like *FIT*, *PYE* may require other bHLH proteins as binding partners to interact with downstream targets. Yeast two hybrid, bimolecular fluorescence complementation, and pulldown analyses have demonstrated that *PYE* can interact with bHLH104, bHLH115, and bHLH105 or IAA-LEUCINE RESISTANT 3 (*ILR3*), three bHLH transcription factors belonging to bHLH subclade IVc (of which only

1
2
3 *bHLH115* has increased expression under Fe-deficiency)²⁰⁻²⁴. By coexpression analysis with
4 *PYE*, a gene encoding a RING E3 ligase with three hemerythrin/HHE Fe-binding domains called
5 *BRUTUS (BTS)* was also classified into this network. BTS is thought to act indirectly with *PYE*
6 because although it does not itself interact with *PYE*, it interacts with the same three IVc bHLH
7 transcription factors as *PYE*²⁰. BTS was subsequently demonstrated to be a functional RING E3
8 ligase *in vitro*, and although it has not been confirmed *in planta*, the three IVc bHLH
9 transcription factors are proposed as targets for proteasomal degradation after ubiquitination by
10 BTS²³. Two of these putative targets, bHLH104 and ILR3 (bHLH105), were recently identified
11 as positive regulators of the Fe deficiency response because loss-of-function mutants exhibit
12 decreased tolerance to Fe deficiency²². Further, bHLH104 and ILR3 regulate downstream
13 expression of *bHLH38/39/100/101* and *PYE*, genes from both the *FIT* and *PYE* networks²². *bts*
14 knockdown mutants, on the other hand, exhibit increased tolerance to Fe deficiency and thus
15 negatively regulate Fe uptake^{20,22,23}. While a full length *BTS* construct can complement *bts-1*
16 mutant phenotypes under low Fe conditions, a deletion construct lacking the RING domain fails
17 to complement the mutant, suggesting the E3 ligase activity of BTS is critical for BTS'
18 repressive role in the Fe deficiency response²⁵. Interestingly, complete loss-of-function *bts*
19 mutants exhibit embryo lethality²⁶. Taken together, current data suggests a model where BTS
20 acts as a negative regulator by targeting transcription factors important in positive regulation of
21 the Fe deficiency response for degradation.

22
23
24
25
26
27
28
29
30
31
32
33
34
35
36
37 Understanding the balance between positive and negative regulation of the Fe deficiency
38 response is essential for efforts to engineer plants with more Fe that do not experience Fe
39 toxicity. Although plants are often challenged with Fe deficiency, no environment remains
40 constant and Fe availability in the rhizosphere depends on many factors. When sufficient Fe is
41 available, it is crucial for plants to effectively suppress the Fe deficiency response to avoid
42 excessive uptake.

43
44
45
46
47 We found that in addition to BTS, two closely related RING E3 ligases that we named
48 BRUTUS LIKE1 and BRUTUS LIKE2 are important in negative regulation of the Fe deficiency
49 response. The double *bts11 bts12* mutant has increased Fe concentrations and tolerance to Fe
50 deficiency compared to wild type and the triple *bts-1 bts11 bts12* mutant has even higher
51 concentrations of Fe and tolerance to Fe deficiency, but without excessive Fe accumulation
52 leading to Fe toxicity. Additionally, we identified a novel allele of *BTS* in a mutagenesis screen
53
54
55
56
57
58
59
60

1
2
3 for altered Fe accumulation. This mutant, *bts-3*, contains a point mutation in the RING E3 ligase
4 domain of BTS, suggesting its E3 ligase activity may be impaired. We sought to explore the
5 unique nature of this missense mutant compared to the other *bts* mutants, which are either
6 embryo lethal or have a reduction in steady-state transcript levels and likely represent partial-
7 loss-of BTS function. *bts-3* is more tolerant than wild type to Fe-deficient conditions. Further,
8 *bts-3* is sensitive to Fe-sufficient conditions and accumulates excessive Fe. Using microarray
9 analysis, we demonstrated that these *bts-3* phenotypes are associated with expression of the Fe
10 deficiency response in the root under both Fe-sufficient and Fe-deficient growth conditions,
11 despite accumulation of high concentrations of Fe in the root. Our characterization of *bts11*,
12 *bts12*, and *bts* mutants increases our understanding of the role of BTS family members as
13 negative regulators of the Arabidopsis Fe deficiency response.
14
15
16
17
18
19
20
21
22
23

24 Results

25 Identification of two *BTS* paralogs in Arabidopsis

26 To determine if there are any other proteins which may play a similar or overlapping role
27 to BTS, we used the Ensembl Plants bioinformatics tool to identify genes encoding proteins in
28 Arabidopsis containing both putative hemerythrin and RING domains²⁷. This analysis identified
29 two *BTS* paralogs, *At1g74770* (*BTSL1*) and *At1g18910* (*BTSL2*) (Figure 1A). Using an amino
30 acid alignment and identity matrix calculated by ClustalW of the proteins encoded by *BTS*,
31 *BTSL1* and *BTSL2*, we determined that *BTSL1* and *BTSL2* exhibit 72% amino acid identity and
32 *BTSL1* and *BTSL2* each have 38% amino acid identity with *BTS*²⁸. Analysis of domain
33 architecture predicted by NCBI CD-Search revealed that while *BTS* contains three putative
34 hemerythrin domains, *BTSL1* and *BTSL2* each contain two (Figure 1A)²⁹. Each E3 ligase also
35 contains a C-terminal Zf-CHY, RING, and Zinc ribbon domain. The RING domain of each
36 protein has a conserved octet of Cys and His residues that form a canonical C3H2C3 RING
37 structure for Zn²⁺ coordination and predicted RING E3 ligase enzymatic activity (Figure 1A).
38 These proteins were also identified in a phylogenetic analysis of hemerythrin domain containing
39 proteins in a study examining the role of the *BTS* orthologs in rice, *Oryza sativa* Hemerythrin
40 motif-containing Really Interesting New Gene (RING)- and Zinc-finger proteins 1 and
41 2 (*OsHRZ1* and *OsHRZ2*)³⁰.
42
43
44
45
46
47
48
49
50
51
52
53
54
55
56
57
58
59
60

1
2
3 All three genes of the *BTS* family in *Arabidopsis* exhibit significantly increased
4 expression in roots of plants exposed to Fe-deficient conditions compared to those grown under
5 Fe-sufficient conditions (Figure 1B). *BTS* and *BTSL2* are expressed at similar levels in the roots
6 and both exhibit approximately a 3-fold increase in expression in Fe-deficient conditions
7 compared to Fe-sufficient conditions. *BTSL1*, on the other hand, exhibits an 8-fold increase in
8 expression in Fe-deficient conditions. In the shoot, we found significant expression of *BTS*,
9 which, like in roots, is increased in response to Fe-deficient growth conditions (approximately a
10 16-fold induction) (Figure 1B). *BTSL1* and *BTSL2* were not significantly expressed in shoots,
11 regardless of Fe status.
12
13
14
15
16
17
18
19
20

21 **Knockdown of *BTS* family E3 ligases increases tissue Fe concentrations and tolerance to Fe** 22 **deficiency**

23
24 A previously identified *bts-1* T-DNA insertion mutant has steady state mRNA levels 70%
25 of those in wild type, and is more tolerant to Fe deficiency than wild type^{20,23}. Because *BTSL1*
26 and *BTSL2* are also expressed under Fe-deficient conditions in the root, we wanted to determine
27 if loss of *BTSL1* and *BTSL2* would affect tolerance to Fe deficiency. We obtained T-DNA
28 insertion lines for each gene (Supplemental Figure 1A). The T-DNA insertion in exon two of
29 *BTSL1* in SALK_015054 results in complete loss of full-length *BTSL1* transcript (Supplemental
30 Figure 1B). In *BTSL2*, sequencing revealed that although the entire open reading frame is
31 present, the T-DNA insertion in SAIL_615_H01 results in a chimeric transcript containing
32 segments of T-DNA, promoter, and the 5'UTR fused upstream of the *BTSL2* open reading frame.
33 This chimeric transcript contains several alternative start sites, making it unlikely that the native
34 translation product is produced in this line (Supplemental Figure 1B).
35
36
37
38
39
40
41
42
43

44 Compared to wild type shoots which exhibit chlorosis when grown under Fe-deficient
45 conditions, *bts-1* plants were greener and contained significantly more chlorophyll (a 44%
46 increase compared to wild type) (Figure 2A), and as demonstrated previously, had longer roots
47 than wild type when grown vertically under Fe-deficient growth conditions (Supplemental
48 Figure 2A). By the same parameters, *bts11* and *bts12* single mutants were indistinguishable from
49 wild type (Figure 2A, Supplemental Figure 2A). However, due to their high amino acid identity,
50 we hypothesized that *BTSL1* and *BTSL2* function redundantly and thus we generated the double
51 *bts11 bts12* mutant. Like *bts-1*, *bts11 bts12* had greener shoots, higher chlorophyll levels (a 92%
52
53
54
55
56
57
58
59
60

1
2
3 increase compared to wild type), and increased root length when plants were grown under Fe-
4 deficient conditions (Figure 2A, Supplemental Figure 2A) compared to wild type. Further, *bts-1*
5 and the *bts11 bts12* double mutant had significantly higher Fe concentrations in roots (65% and
6 78% respectively) and shoots (33% and 25% respectively) of plants grown under Fe-sufficient
7 conditions compared to wild type (Figure 2C). To assess whether both reduction of *BTS* and loss
8 of *BTSL1* and *BTSL2* expression can further increase Fe content and tolerance to Fe deficiency,
9 we created the triple *bts-1 bts11 bts12* mutant. Compared to the single *bts-1* mutant and the *bts11*
10 *bts12* double mutant alone, the triple *bts-1 bts11 bts12* mutant exhibited additional tolerance to Fe
11 deficiency as seen by visibly greener shoots, significantly increased chlorophyll concentrations
12 (236% increase compared to wild type), and longer roots when plants were grown on Fe-
13 deficient conditions (Figure 2A, Supplemental Figure 2A). The triple mutant also had
14 significantly higher Fe concentrations in roots and shoots of plants grown under both Fe regimes
15 compared to wild type (Figure 2C). In addition, we found that triple mutant seeds have
16 significantly higher concentrations of Fe than wild type (32% increase) (Figure 2D). Imaging Fe
17 *in situ* in intact seeds revealed that although seed Fe concentrations are increased significantly in
18 the triple mutant, Fe localization is not perturbed from wild type and is associated with the
19 embryonic vasculature as previously described (Figure 2E) ³¹.
20
21
22
23
24
25
26
27
28
29
30
31
32
33
34

35 **Increased Fe concentrations and storage in these mutants is not associated with Fe toxicity**

36
37 Because increased Fe accumulation can be toxic to plants, we assessed *bts11*, *bts12*, *bts-1*,
38 *bts11 bts12*, and *bts-1 bts11 bts12* for signs of Fe toxicity, such as stunted root growth or necrosis,
39 when plants were grown under Fe-sufficient conditions. None of these mutants appeared
40 different from wild type under these conditions (Supplemental Figure 2B). Thus, increased Fe
41 concentrations in these mutants enhances tolerance to Fe-deficient growth conditions, but does
42 not negatively impact growth under Fe-sufficient conditions. Because of this, we were interested
43 in where these mutants store Fe to detoxify it. To address this question, we imaged Fe *in vivo* in
44 intact leaves of our mutants compared to wild type plants grown under Fe-sufficient conditions.
45 This *in vivo* elemental imaging also demonstrated increased Fe levels in mutants (Figure 2B),
46 supporting data obtained by the bulk quantification of Fe concentrations in digested whole leaves
47 (Figure 2B and Figure 2C). From a two-dimensional perspective, in wild type, *bts11* and *bts12*
48 single mutants, Fe is distributed relatively evenly throughout the leaf surface with some
49
50
51
52
53
54
55
56
57
58
59
60

1
2
3 enrichment in the main vein and in trichomes. In *bts-1* and *bts11 btsl2*, Fe accumulation is
4 increased throughout the leaf, the central vein, and trichomes compared to wild type. The triple
5 mutant exhibits a further increase in Fe throughout the leaf compared to *bts-1* and *bts11 btsl2* and
6 increased enrichment of Fe in the central vein and trichomes and in minor veins (Figure 2B).
7 These data suggest these regions are sites of Fe accumulation/storage in Arabidopsis leaves.
8
9

10
11
12 Elemental imaging of leaves from plants grown under Fe-deficient conditions
13 demonstrates that in wild type, trichomes are depleted of Fe and no enrichment can be seen in the
14 main vein as in plants grown under Fe-sufficient conditions (Figure 3 top panel). The double
15 mutant has less Fe in the trichomes of plants exposed to Fe-deficient conditions compared to Fe-
16 sufficient conditions, but still contains Fe in trichomes and the main vein, which is not seen in
17 wild type (Figure 2B and Figure 3). In agreement with increased total leaf Fe concentrations
18 (Figure 2C), the triple mutant has even more Fe in the trichomes, the main vein, and throughout
19 the leaf tissue compared to the double mutant (Figure 3).
20
21
22
23
24
25
26
27

28 ***BTS* family E3 ligase mutants also have increased concentrations of other metals**

29
30 Because metals share and compete for uptake transporters, we wanted to determine if our
31 mutants had higher concentrations of other essential micronutrient metals, particularly those
32 transported by IRT1: Zn and Mn^{8,32}. We found that in roots, the double *bts11 btsl2* and triple
33 *bts-1 bts11 btsl2* mutants had significantly higher Zn concentrations compared to wild type and
34 *bts-1* (Supplemental Figure 3A). In shoots, the double and triple mutants had significantly higher
35 concentrations of Zn compared to wild type and *bts-1* and the triple mutant had significantly
36 higher concentrations of Mn compared to wild type, *bts-1*, and *bts11 btsl2* (Supplemental Figure
37 3A). None of the mutants had elevated concentrations of Cu, a metal not transported by IRT1, in
38 either roots or shoots. In seeds, we found significantly higher concentrations of Mn and Zn in
39 *bts-1*, *bts11 btsl2*, and *bts-1 bts11 btsl2* compared to wild type (51%, 35%, and 46% increases of
40 Mn compared to wild type, respectively and 22%, 36%, and 60% increases of Zn compared to
41 wild type, respectively) (Supplemental Figure 3B).
42
43
44
45
46
47
48
49
50

51 We imaged Zn and Mn *in vivo* in intact leaves in shoots of the double and triple mutants
52 compared to wild type (Figure 3 middle and bottom panels). We found that in wild type leaves,
53 Zn enrichment is mainly found in hydathodes and veins. In *bts11 btsl2* and *bts-1 bts11 btsl2*
54 mutants, Zn accumulates in the hydathodes, and more is seen in the veins and at the base of
55
56
57
58
59
60

1
2
3 trichomes. Mn is found mainly at the base of the trichomes in wild type and in the double and
4
5 triple mutants, it can be seen in the stalk and branches of trichomes. These increases we see in Zn
6
7 and Mn at specific sites in the leaf are in agreement with the increases in Zn and Mn
8
9 concentrations we observe in digested whole leaf samples (Supplemental Figure 3A).

12 **Identification of *bts-3*, an Fe overaccumulating *BTS* mutant**

14 In an attempt to uncover additional regulators of the Fe deficiency response, we screened
15 leaves from over 6,000 EMS mutagenized Arabidopsis plants following a high throughput
16 elemental profiling approach we previously used³³ to successfully identify mutants with altered
17 elemental profiles (*aka* ionome)³⁴⁻³⁸. In this screen, we identified a mutant that accumulated
18 significantly more Fe than wild type. The mutant was backcrossed twice and the mutation
19 determined to be recessive. Bulk segregant analysis with microarray-based detection of genetic
20 markers on phenotyped pools of F2 plants from a *bts-3* x Ler outcross, following our previously
21 developed approach³⁹⁻⁴¹, placed the causal mutation in a 1 Mb interval centered at 6 Mb on
22 chromosome 3. Fine mapping of F2 recombinants using SNP-based markers was used to narrow
23 down the mutation to a region of chromosome 3 between 6237000 and 6342000. Sequencing in
24 this region revealed a C to T mutation at base pair 5753 of *BTS* genomic DNA. The single base
25 pair change in this *bts-3* mutant confers a Pro to Leu change at amino acid 1174 in the RING
26 domain of BTS (Figure 1A).
27
28
29
30
31
32
33
34
35
36

37 Elemental analysis revealed that *bts-3* contained significantly higher concentrations of Fe
38 in roots and shoots when grown under Fe-sufficient and Fe-deficient conditions compared to
39 wild type confirming the results obtained in the original screen (Figure 4A). *bts-3* seeds have Fe
40 concentrations that are more than double than those of wild type, (a 244% increase) compared to
41 the 32% increase in seed Fe of the *bts-1 bts1 btsl2* triple mutant compared to wild type (Figure
42 4A, Figure 2D). *bts-3* also had significantly higher concentrations of Fe in roots of plants grown
43 under Fe-sufficient conditions and in shoots of plants grown under both Fe conditions compared
44 to the triple mutant (Figure 2C and Figure 4A). We also performed *in vivo* elemental imaging on
45 intact tissues and we found that increased Fe accumulation occurs in both roots and shoots in *bts-*
46 *3* compared to wild type (Figure 4B-C), confirming our analysis of the total Fe concentration in
47 whole roots and leaves (Figure 4A). In roots, where Fe uptake from the rhizosphere occurs, Fe in
48 wild type was mainly localized to a distinct portion of the root meristem, perhaps the quiescent
49
50
51
52
53
54
55
56
57
58
59
60

1
2
3 center (Figure 4B). In *bts-3* roots, however, Fe was dispersed beyond this region in puncta,
4 which may represent vacuolar Fe storage sites. In Fe-sufficient leaves, Fe was also greatly
5 increased, particularly in the vasculature (including the central vein and minor veins) and
6 trichomes (Figure 4C). We also examined *bts-3* alongside the previously imaged Fe-deficient
7 leaves and found that *bts-3* leaves have increased Fe storage in trichomes and throughout the leaf
8 tissue compared to the double and triple mutants (Figure 3). Because our two-dimensional
9 analysis revealed an increase in Fe associated with the vasculature in *bts-3*, we wanted to
10 determine where Fe accumulates at the cellular level. Elemental imaging of manually cross-
11 sectioned primary vasculature revealed that *bts-3* has higher levels of Fe in phloem compared to
12 wild type (Figure 4E). Finally, *in vivo* elemental imaging of seeds within green siliques and of
13 dry seed demonstrated that Fe is associated with the vasculature of the embryo at a much higher
14 concentration in *bts-3* seed compared to wild type (Figure 4D, Figure 4F). Higher resolution
15 elemental imaging reveals that Fe also accumulates in the seed coat of *bts-3* (Figure 4F).
16
17
18
19
20
21
22
23
24
25
26
27

28 ***bts-3* also accumulates high concentrations of other metals**

29
30 We wanted to determine if *bts-3* had increased concentrations of other metals in addition
31 to Fe. Bulk analysis of digested whole leaves revealed increases in Mn and Zn concentrations
32 compared to wild type in both roots and shoots of *bts-3* plants (Supplemental Figure 3A).
33 Compared to the triple mutant, *bts-3* had similar concentrations of Zn in roots and shoots, but
34 significantly higher concentrations of Mn in both tissues (Supplemental Figure 3A). In
35 comparison with our *in vivo* imaging of Zn and Mn accumulation in shoots, we found that like
36 the triple mutant, *bts-3* had Zn enrichment in the veins, hydathodes, and at trichome bases
37 (Figure 3). *bts-3* trichomes had higher levels of Mn compared to trichomes of the triple mutant
38 (Figure 3). In seeds, *bts-3* had significantly higher concentrations of Mn and Zn compared to
39 wild type (Supplemental Figure 3C). We note that concentrations of Mn and Zn in wild type
40 seeds were different for seeds shown in Supplemental Figure 3B compared to Supplemental
41 Figure 3C. This is likely due to variation in metal content of the soil and/or water, as these
42 experiments were performed independently.
43
44
45
46
47
48
49
50
51
52

53 ***bts-3* is sensitive to Fe supply, but thrives in Fe-deficient conditions**

54
55 We next examined the effect of increased Fe accumulation in *bts-3* plants grown under
56 Fe-deficient and Fe-sufficient conditions. When *bts-3* plants were grown on normal, Fe-
57
58
59
60

1
2
3 sufficient soil, they were smaller than wild type and *bts-1* plants (Figure 5A). However, when
4 plants were grown on Fe-deficient alkaline soil, both *bts-1* and *bts-3* plants were larger and
5 greener than wild type, which is small and chlorotic. The chlorosis that developed in wild type
6 plants grown on alkaline soil could be rescued by watering plants with exogenous Fe. However,
7 when *bts-1* and *bts-3* plants were watered with the same amount of Fe, *bts-3* plants did not grow
8 beyond the seedling stage, while *bts-1* plants were visibly unaffected by Fe addition. In addition,
9 we observed that *bts-3* had visibly shorter roots and small shoots compared to wild type plants
10 grown on Fe-sufficient plates (Figure 5B). Although our bulk and imaging analyses of Fe
11 revealed increased shoot Fe concentrations of *bts-1* plants grown under Fe-sufficient conditions
12 (Fig 2C & Figure 5C), *bts-1* did not display the short root phenotype, highlighting the unique
13 phenotype of *bts-3* (Figure 5B, See also Supplemental Figure 2B for comparison to previously
14 discussed mutants of this study). On the other hand, in Fe-deficient conditions, *bts-3* grew longer
15 roots than wild type (Figure 5A, Supplemental Figure 2A), similar to *bts-1* mutants.

16
17 We could restore to wild type levels *bts-3* Fe sensitivity, leaf size, and Fe
18 levels/localization when we transformed the mutant with a complementation construct containing
19 the wild type Col-0 allele of *BTS* driven by its native promoter, which we named *ProBTS:BTS*
20 *bts-3* (Figure 5C-D). This complementation line confirmed that the recessive mutation in *BTS* is
21 responsible for the Fe-related phenotypes of *bts-3*. Mn and Zn were also restored to wild type
22 levels and distribution patterns in complemented lines (Supplemental Figure 4).

23 ***bts-3* roots exhibit the Strategy I Fe deficiency response regardless of Fe growth** 24 **conditions**

25 Because *bts-3* accumulates more Fe than wild type, experiences Fe toxicity when grown
26 under Fe-sufficient conditions, and thrives in Fe-deficient conditions, we hypothesized that *bts-3*
27 has a constitutively active Fe deficiency response. At the transcriptional level, *bts-3* exhibits
28 increased expression of *FRO2* and *IRT1* in Fe-sufficient conditions compared to WT and
29 decreased expression in Fe-deficient conditions compared to WT (Figure 6A). Assays of ferric-
30 chelate reductase activity showed that unlike wild type, where significant Fe reduction occurred
31 only in Fe-deficient conditions, *bts-3* reduced Fe³⁺ regardless of Fe status (Figure 6B). We also
32 examined ferric chelate reductase activity in the *bts-1 bts11 bts12* Fe accumulating triple mutant;
33 although we see an increase in ferric chelate reductase activity in Fe-deficient conditions
34 compared to wild type, there is no increase in Fe reduction in the triple mutant in Fe-sufficient
35
36
37
38
39
40
41
42
43
44
45
46
47
48
49
50
51
52
53
54
55
56
57
58
59
60

1
2
3 conditions compared to wild type (Supplemental Figure 5). By western blotting, we showed that
4 in wild type, IRT1 protein is only present in Fe-deficient conditions (Figure 6C). In *bts-3*
5 however, IRT1 protein accumulation occurs in Fe-sufficient conditions as well as in Fe-deficient
6 conditions. Although this IRT1 accumulation in *bts-3* plants grown under Fe-sufficient
7 conditions is aberrant compared to wild type, IRT1 protein levels still exhibit Fe regulation
8 because concentrations in Fe-deficient conditions are higher than concentrations in Fe-sufficient
9 conditions.
10
11
12
13
14
15

16 17 18 **The *bts-3* transcriptome varies dramatically from wild type**

19 Because we found the Fe uptake response to be active in *bts-3* roots regardless of Fe
20 status, we wanted to understand at what level BTS might be acting, i.e. how upstream BTS acts
21 and if *BTS* misregulation affects only a subset or multiple subsets of Fe-regulated genes. We
22 were also interested in studying the transcriptome of the *bts-3* mutant to determine how
23 high/toxic Fe concentrations influence gene expression. To address these questions, we
24 performed a microarray analysis comparing roots of wild type to *bts-3* plants exposed to either
25 Fe-sufficient or Fe-deficient growth conditions. We performed hierarchical clustering analysis on
26 genes that were at least 1.5-fold upregulated or downregulated by Fe in either wild type or
27 mutant. From top to bottom of heat map (Figures 7), four major defined subsets of genes were
28 found in the cluster analyses: 1) genes which were more highly expressed in Fe-sufficient
29 conditions compared to Fe-deficient conditions in wild type, 2) genes which were more highly
30 expressed in *bts-3* in Fe-sufficient conditions compared to all other genotypes/treatments, 3)
31 genes which were expressed at lower levels in *bts-3* Fe-sufficient conditions compared to other
32 genotypes/treatments, and 4) genes which were more highly expressed in Fe-deficient conditions
33 compared to Fe-sufficient conditions in wild type (Figure 7). We also performed Gene Ontology
34 (GO) term enrichment analysis on each of these subsets to understand general features of *BTS*
35 misregulation^{42, 43}. We will briefly discuss major findings of each subset that are most relevant
36 to our understanding of the role of *BTS* in Fe homeostasis.
37
38
39
40
41
42
43
44
45
46
47
48
49
50
51
52

53 **Subset 1: Genes upregulated in Fe-sufficient wild type roots exhibited reduced expression** 54 **in Fe-sufficient *bts-3* roots** 55 56 57 58 59 60

1
2
3 The subset of genes that were more highly expressed in the roots in Fe-sufficient
4 conditions compared to Fe-deficient conditions in wild type were enriched in the following GO
5 terms: Fe ion homeostasis, oxidation/reduction, and transition metal binding. In general,
6 expression of these genes was not increased to reflect higher Fe levels in *bts-3* (Figure 7).
7 Included in this subset of genes were *FERREDOXIN (FEDA)*, *STROMAL ASCORBATE*
8 *PEROXIDASE, (SAPX)*, and *FERRITIN, (FER4)* (encoding the major Fe storage protein, FER).
9 Although *bts-3* roots contained significantly more Fe than wild type roots in Fe-sufficient
10 conditions, expression of many Fe sufficiency induced genes within this subset did not increase
11 accordingly and were actually reduced compared to wild type. When plants were grown on Fe-
12 deficient medium, expression of the genes within this subset was low in wild type roots, but
13 slightly increased in *bts-3* roots, which corresponded to the higher Fe concentration in *bts-3* roots
14 compared to wild type roots under Fe deficiency. However, *bts-3* roots grown under Fe
15 deficiency still contained more Fe than wild type roots under Fe sufficiency, and expression of
16 these genes did not reach wild type levels. As a whole, the *bts-3* root did not display an Fe-
17 sufficient gene expression profile that corresponded simply with its Fe status.
18
19
20
21
22
23
24
25
26
27
28
29
30
31

32 **Subsets 2 and 3: High concentrations of Fe in *bts-3* roots corresponded with major** 33 **transcriptional remodeling in Fe-sufficient conditions**

34
35 There were a large number of genes that did not exhibit strong changes in expression
36 levels in response to Fe treatment in wild type and were expressed at similar levels to wild type
37 in *bts-3* grown under Fe-deficient conditions but had increased expression in *bts-3* grown under
38 Fe-sufficient conditions (Figure 7, Subset 2). Enriched GO terms included response to metal ion,
39 cell wall, glutathione-S-transferases, and response to oxidative stress. Included in this subset
40 were known metal homeostasis genes, including genes encoding Fe transporters called
41 *NATURAL RESISTANCE-ASSOCIATED MACROPHAGE PROTEIN 3 (NRAMP3)* and *FERRIC*
42 *REDUCTASE DEFECTIVE 3 (FRD3)*, an Al transporter *ALUMINUM-ACTIVATED MALATE*
43 *TRANSPORTER 1 (ALMT1)*, a Pb transporter *PLEIOTROPIC DRUG RESISTANCE 12*
44 *(PRD12)*, and the gene encoding the enzyme for synthesis of the Fe chelator nicotianamine,
45 *NICOTIANAMINE SYNTHASE 2 (NAS2)*.
46
47
48
49
50
51
52
53
54

55 Subset 3 includes genes that were relatively unchanged by Fe status in wild type and
56 expressed at similar levels to wild type in *bts-3* Fe-deficient plants, but significantly
57
58
59
60

1
2
3 downregulated in *bts-3* Fe-sufficient roots (Figure 7). The significantly enriched GO term in this
4 subset was endomembrane system.
5
6
7

8 **Subset 4: *bts-3* roots expressed Fe deficiency responsive genes regardless of Fe status**

9
10 In subset 4, many genes that were induced only in Fe-deficient conditions in wild type
11 were expressed in *bts-3* roots grown under both Fe regimes (Figure 7, Supplemental Figure 6A).
12 In most cases, expression of these genes did not reach the level of induction seen in wild type Fe-
13 deficient roots, but they were still elevated compared to wild type Fe-sufficient roots. Further,
14 many of the Fe deficiency responsive genes exhibited dampened expression in *bts-3* roots
15 compared to wild type roots in plants grown under Fe-deficient conditions. In addition, *bts-3* Fe-
16 deficient roots showed increased expression of these genes in Fe-deficient conditions compared
17 to *bts-3* roots in Fe-sufficient conditions. Taken together, this indicates that *bts-3* roots did have
18 some ability to regulate transcription in response to Fe status, but it was still greatly perturbed
19 compared to wild type because roots were unable to completely repress gene expression in Fe-
20 sufficient conditions as wild type roots did. For example, two known upstream Fe deficiency
21 responsive genes, *FIT* and *PYE*, encoding bHLH transcription factors, exhibited increased
22 expression in *bts-3* Fe-sufficient conditions compared to wild type. Similarly, other transcription
23 factors involved in the Fe deficiency response that are normally induced only under Fe
24 deficiency also showed expression in roots of *bts-3* plants grown under Fe-sufficient conditions.
25 These were *bHLH38*, *bHLH39*, *bHLH100*, *bHLH101*, *MYB10*, and *MYB72*. *FIT* is required for
26 activation of downstream targets *FRO2* and *IRT1*, which as previously mentioned are responsible
27 for Fe reduction and uptake in the root. These genes were also induced in *bts-3* Fe-sufficient
28 roots. *PYE* targets *FRO3* and *ZIF1* were also constitutively activated in *bts-3*. The downstream
29 targets of *MYB10* and *MYB72*, *NAS2* and *BETA GLUCOSIDASE 42 (BGLU42)*, were also
30 induced regardless of Fe status in the *bts-3* mutant. Other Fe deficiency responsive genes that
31 were activated in Fe-sufficient conditions in *bts-3* included *NRAMP1*, *NRAMP4*, *IRT2*, *ZIP8*,
32 *COPPER TRANSPORTER 2 (COPT2)*, *IRON REGULATED 2 (IREG2)*, *OBP3-RESPONSIVE*
33 *GENE 1 (ORG1)*, and *HEAVY METAL ATPASE 3 (HMA3)*. Finally, *BTS* itself and *BTSL1* and
34 *BTSL2* were also expressed in *bts-3* roots regardless of Fe status. Only a small number of Fe
35 deficiency responsive genes exhibited normal expression in *bts-3* roots, such as *At1g47400* and
36
37
38
39
40
41
42
43
44
45
46
47
48
49
50
51
52
53
54
55
56
57
58
59
60

1
2
3 *At3g56360*, but the function of these genes is currently unknown. Select bHLH TFs were
4 analyzed by qPCR to validate the results of the microarray (Supplemental Figure 6B).
5
6
7

8 **Discussion**

9 **Characterization of *BTS* paralogs in the Fe deficiency response**

10 We characterized the role of two new E3 ligases in the Fe-deficiency response, BTSL1
11 and BTSL2. We found that like *BTS*, *BTSL1* and *BTSL2* were expressed in roots of plants grown
12 under Fe-deficient conditions. Single *bts11* and *bts12* mutants did not exhibit any Fe phenotypes
13 compared to wild type, suggesting a redundant function for these two highly related E3 ligases.
14 Because of this, we made a *bts11 bts12* double mutant and found increased Fe levels and
15 increased tolerance to Fe deficiency compared to wild type. To assess whether reduction of *BTS*
16 expression in the previously identified *bts-1* mutant could further increase Fe content and
17 tolerance to Fe deficiency in *bts-1 bts11 bts12* plants, we created the *bts-1 bts11 bts12* triple mutant. This
18 triple mutant indeed exhibited a further increase in Fe levels and tolerance to Fe deficiency,
19 without any resulting Fe toxicity. Overall, these results demonstrate the importance of these three
20 E3 ligases in the regulation of the Fe-deficiency response. As noted, all three genes exhibited
21 increased expression in Fe-deficient conditions compared to Fe-sufficient conditions in roots,
22 while only *BTS* was significantly expressed in Fe-deficient conditions in the shoots. Future
23 studies should further examine the unique role of *BTS* in shoots.
24
25
26
27
28
29
30
31
32
33
34
35
36
37
38

39 **Identification of a novel *BTS* allele**

40 In our screen for plants with altered Fe concentrations, we identified a *bts* mutant with a
41 novel phenotype. Previous *bts* alleles *emb2454-1* and *emb2454-2* were identified in a screen for
42 essential genes in Arabidopsis and exhibited embryo lethality and are thus putative complete
43 loss-of-function alleles²⁶. To date, only partial loss-of-function alleles have been used to
44 examine the role of *BTS* in post-embryonic development. The *bts-1* line exhibits a steady state
45 level of *BTS* mRNA approximately 70% that of wild type when grown under Fe-sufficient
46 conditions. In *bts-1*, normal *BTS* protein is predicted, but at lower levels. *bts-3* has a proline to
47 leucine mutation at amino acid 1174 in the *BTS* RING domain. Our data suggests this protein
48 variant is perturbed in its function, resulting in a phenotype distinct from the reduction in
49
50
51
52
53
54
55
56
57
58
59
60

1
2
3 function of BTS found in the *bts-1* mutant. This unique mutant allowed us to further explore the
4 role of BTS.
5
6
7

8 9 **Possible models for BTS action in the root**

10 The fact that *bts-3* performs better in Fe-deficient conditions compared to wild type
11 supports the idea that BTS is a negative regulator of the Fe deficiency response. Given that BTS
12 is an E3 ligase, it is likely that BTS acts in the ubiquitin-dependent degradation of positive
13 regulator(s) of the Fe deficiency response, as has been suggested previously^{22, 23, 25}. Because
14 BTS is an E3 ligase containing Fe-binding hemerythrin domains, we were interested in whether
15 it acts in a similar manner to the Fe sensor identified in mammals, FBXL5. *FBXL5* mRNA
16 exhibits constitutive expression, but FBXL5 protein stability is controlled by Fe binding to the
17 hemerythrin domains, where Fe binding stabilizes FBXL5 protein so that it can assemble with
18 other subunits to form a complete SCF ubiquitin ligase and perform its function to ubiquitinate
19 IRP2, leading to proteasomal degradation of IRP2^{44, 45}. In low Fe conditions, the hemerythrin
20 domain is destabilized, resulting in FBXL5 degradation. If BTS acts in an analogous manner, Fe
21 binding to hemerythrin domains would stabilize BTS protein, allowing for its activity in Fe-
22 sufficient conditions (Figure 8). If target proteins are positive regulators of the Fe deficiency
23 response, BTS could degrade these regulators when Fe becomes available after a period of Fe
24 deficiency. The expression of *BTS* in Fe-deficient conditions would allow for a quick transition
25 to Fe availability via Fe-mediated BTS protein stabilization. This could allow a rapid “switching
26 off” of the Fe deficiency response when Fe uptake is no longer needed. In a scenario where BTS
27 protein is mutated so that it is unstable and/or enzymatically inactive, as we believe to be the
28 case in *bts-3*, a loss of ubiquitin ligase activity would result in lack of degradation of target
29 proteins. Notably, there is strong support in the literature that the Pro to Leu change renders BTS
30 P1174L incapable of interacting with its partner E2 enzyme because the conserved Pro has
31 previously been identified as a residue important for this interaction in specific E2-E3 pairs⁴⁶⁻⁵¹.
32 This hypothesis is outlined in the model shown in Figure 8. Lack of degradation and resulting
33 accumulation of positive regulators of the Fe deficiency response would result in a constitutive
34 activation of the Fe deficiency response and excessive Fe uptake and resulting toxicity, as we see
35 in *bts-3* (Figure 7). This can also explain why *bts-3* performed better than wild type in Fe-
36
37
38
39
40
41
42
43
44
45
46
47
48
49
50
51
52
53
54
55
56
57
58
59
60

1
2
3 deficient conditions. Because *bts-3* plants always take in Fe, even when there is sufficient Fe
4 available for growth, they have stored Fe available when faced with low Fe conditions.
5
6

7 Although protein levels and ubiquitination status of putative BTS targets have not been
8 studied in *bts* mutants *in planta*, protein interaction studies and *in vitro* cell-free degradation
9 experiments suggest that BTS targets may include bLH104, bHLH115, and ILR3^{20,23}. bHLH104
10 and ILR3 have been shown to be positive regulators of the Fe deficiency response because loss-
11 of-function mutants of these genes are sensitive to Fe-deficient conditions²². Further, these
12 transcription factors have been shown to directly bind to promoters and influence expression of
13 Fe deficiency responsive genes: *bHLH38*, *bHLH39*, *bHLH100*, *bHLH101*, and *PYE*²². We show
14 that in *bts-3* roots, these genes and others are expressed regardless of Fe status, supporting the
15 hypothesis that BTS acts upstream to control expression of these genes. As mentioned
16 previously, bHLH1b subgroup transcription factors can form dimers with FIT. We demonstrated
17 that downstream targets of FIT, *IRT1* and *FRO2*, are constitutively expressed and their protein
18 products function to reduce and transport Fe into the root irrespective of Fe status of the plant
19 (Figure 6, Figure 7).
20
21
22
23
24
25
26
27
28
29

30 Besides the possibility that BTS functions in a similar manner to FBXL5 with Fe binding
31 to hemerythrin domains leading to protein stability (Figure 8), another study suggests the
32 opposite is true. Protein stability assays using a wheat germ *in vitro* translation system suggest
33 that BTS is less stable in the presence of Fe and thus the authors propose that BTS is active in
34 Fe-deficient conditions, when *BTS* gene expression is induced²³. This *in vitro* data further
35 suggests that this Fe-dependent destabilization is dependent on specific Fe binding residues
36 within the hemerythrin domains. However, MG132 proteasomal inhibitor sensitivity of this
37 putative protein destabilization was not shown and thus it is difficult to conclude whether BTS
38 degradation is occurring in response to Fe or whether Fe simply negatively regulates the
39 translation of BTS protein in the wheat germ extract system. The authors of this study suggest
40 that if BTS is more stable in Fe-deficient conditions, BTS acts under these conditions to “fine-
41 tune” regulators of the Fe deficiency response²³. A fine-tuning capability may serve to inhibit
42 excessive Fe accumulation by preventing uncontrolled action of positive regulators of the Fe
43 deficiency response. It is well known that Fe levels are tightly controlled because excess Fe can
44 be very toxic to plants and therefore, this idea of fine-tuning is plausible. Alternatively, BTS may
45 function in the constitutive turnover of positive regulators of the Fe deficiency response in order
46
47
48
49
50
51
52
53
54
55
56
57
58
59
60

1
2
3 to keep them “fresh” so they can continually bind to target promoters to activate Fe deficiency
4 responsive genes when processive transcriptional cycles are needed The requirement for “fresh”
5 transcription factor production to replace “fatigued” transcription factors to promote continuous
6 gene expression has been suggested for FIT protein regulation⁵². Alternatively, constant
7 degradation of positive regulators by BTS may be necessary to ensure that once synthesized,
8 positive regulators can be rapidly removed upon Fe resupply to prevent excess accumulation.
9

10
11
12 Unfortunately, we and others have been unable to detect full-length BTS protein in Fe-
13 sufficient vs. Fe-deficient conditions *in planta*, making it difficult to conclude how BTS protein
14 stability/activity is physiologically regulated by Fe availability²³.
15
16
17
18
19

20 21 **Conclusions**

22
23 Considering the models discussed, if a plant is reduced in its ability to fine-tune or
24 appropriately regulate protein stability of positive regulators of the Fe deficiency response in Fe-
25 deficient conditions, an increased activation of the Fe deficiency response and resulting
26 increased tolerance to Fe-deficient conditions may occur. Our *bts-1*, *bts11 bts12*, and *bts-1 bts11*
27 *bts12* mutant phenotypes seem to fit this scenario. Because they probably do not completely lack
28 their BTS E3 ligase activity due to the presence of some full-length *BTS* transcript in these
29 mutants, we propose they retain some capacity to negatively regulate the Fe deficiency response.
30 Proper balance of both positive and negative regulation of the Fe deficiency response is essential,
31 especially from an applied perspective. The triple *bts-1 bts11 bts12* mutant we created represents
32 what we consider an ideal Fe accumulator: it takes in more Fe than wild type to allow for
33 enhanced growth and tolerance to Fe deficiency, but still retains the capacity to sufficiently
34 repress Fe uptake in Fe-sufficient growth conditions to avoid toxicity.
35
36
37
38
39
40
41
42
43

44 *BTS* orthologs are found across many plant species including crop plants such as rice and
45 soybean and thus represent a potential target for enhancing tolerance to Fe deficiency and
46 increasing Fe bioavailability for human consumption. In rice, RNAi knockdown of *BTS*
47 orthologs, the *HRZs*, was demonstrated to increase tolerance to growth on Fe-deficient
48 calcareous soils and increase Fe concentration in seeds without a yield penalty³⁰. Besides
49 genetic knockdowns and modifications, perhaps natural variants of these genes in crop species
50 may be identified and used in traditional breeding efforts to generate cultivars with more Fe. We
51
52
53
54
55
56
57
58
59
60

1
2
3 hope that the work described here will lead to greater understanding of plant Fe homeostasis to
4 inform efforts for improved crops.
5
6

7 8 9 **Experimental Methods**

10 11 12 **Plant growth conditions**

13
14 For plate grown plants, seeds were surface sterilized and stratified for three days at 4°C in
15 the dark. Gamborg's B5 medium (Sigma-Aldrich) was supplemented with 1mM MES, 0.5%
16 sucrose, 0.6% type M agar, and adjusted to pH 5.8. +Fe and -Fe plates were made with
17 macronutrients and micronutrients at 2 mM Ca(NO₃)₂, 0.75 mM K₂SO₄, 0.65 mM MgSO₄, 0.1
18 mM KH₂PO₄, 10 μM H₃BO₃, 0.1 μM MnSO₄, 0.05 μM CuSO₄, 0.05 μM ZnSO₄, 0.005
19 μM (NH₃)₆Mo₇O₂₄, 1mM MES, 0.6% agar, adjusted to pH 6.0 and supplemented with either 50
20 μM Fe(III)-EDTA for +Fe plates or 300 μM ferrozine [3-(2-pyridyl)-5,6-diphenyl-1,2,4-triazine
21 sulfonate (HACH Chemical)] for -Fe plates as described^{53,54}. Alkaline soil was generated by
22 adding approximately 7.8 gm CaO/kg soil to achieve a soil pH of 7.5-8. To supplement plants
23 grown on alkaline soil, 500 μM FeEDDHA was added. All plants in this study were grown at
24 21°C under a 16 hour light/8 hour dark cycle.
25
26
27
28
29
30
31
32
33

34 35 **Mutant lines**

36
37 *BTS/At3g18290 (bts-1)*, *BTSL1/At1g74770 (bts1l)*, and *BTSL2/At1g18910 (btsl2)* T-
38 DNA insertion lines were obtained from ABRC (SALK_016526, SALK_015054,
39 SAIL_615_HO1, respectively). Homozygous lines were identified using gene-specific primers
40 and a T-DNA specific border primer. Location of T-DNA insertions are shown in Supplemental
41 Figure 1. *bts-3* was identified in an EMS mutagenesis screen and backcrossed twice. *bts1l btsl2*
42 was generated by crossing *btsl* and *btsl2* and identifying a homozygous double mutant. *bts1l*
43 *btsl2* was crossed with *bts-1* to generate the *bts-1 bts1l btsl2* mutant and a homozygous triple
44 mutant was identified.
45
46
47
48
49
50
51
52

53 **Array Mapping**

54
55 The Fe over accumulating mutant was crossed to Ler and F2 plants were scored for
56 sensitivity to Fe sufficient growth conditions. Two pools of plants were created, one with the Fe
57
58
59
60

1
2
3 sensitivity mutant phenotype and one with the wild type phenotype. DNA extracted from the two
4 pools was hybridized to the AtSNPTile array and the mapping was performed as described in
5 Becker et al.³⁹. The array files are available on GEO.
6
7
8
9

10 **Plasmid construction and plant transformation**

11
12 The endogenous promoter complementation line was generated by amplifying the region
13 including 1.9 kb upstream of the *BTS* ATG and the entire *BTS* gene and is named *ProBTS:BTS*
14 *bts-3*. This construct was subcloned into pCR8 (Invitrogen) and finally into pEARLEY GATE
15 301 using Gateway LR Clonase II (Invitrogen). *Agrobacterium tumefaciens* strain GV3101 was
16 transformed with the above construct and *bts-3* plants were transformed using the floral dip
17 method⁵⁵. Transformants were isolated using BASTA selection at 25 mg/mL.
18
19
20
21
22
23

24 **Chlorophyll assay**

25
26 Plants were grown for 10 days on B5 medium and then transferred to –Fe medium for 7
27 days. The shoots were harvested and assayed for chlorophyll concentration by heating plants in
28 95% ethanol at 80°C as previously described⁵⁶.
29
30
31
32

33 **Elemental concentration analysis**

34
35 Root and shoot tissues were collected from plants and to remove trace surface metals,
36 tissues were incubated for 5 mins in 5 mM CaSO₄, 5 mins in 10 mM EDTA, and rinsed with
37 deionized water. Root and shoot tissues were dried before analysis by incubation in open
38 Eppendorf tubes at 70°C for 24 hours. Seeds were harvested when fully dried. Dry tissues (shoot,
39 root and seed) were transferred into Pyrex test tubes (16 x 100 mm). After weighing the
40 appropriate number of samples (these masses were used to calculate the rest of the sample
41 masses after Danku et al.⁵⁷, trace metal grade nitric acid (J. T. Baker Instra-Analyzed; Avantor
42 Performance Materials; Scientific & Chemical Supplies Ltd, Aberdeen, UK) spiked with indium
43 internal standard was added to the tubes (1.00 mL). They were then digested in dry block heaters
44 (DigiPREP MS, SCP Science; QMX Laboratories, Essex, UK) at 115°C for 4 hours. The
45 digested samples were diluted to 10.0 mL with 18.2 MΩcm Milli-Q Direct water (Merck
46 Millipore, Watford, UK) and aliquots transferred to 96-well deep well plates using adjustable
47 multichannel pipette (Rainin; Anachem Ltd, Luton, UK) for analysis. Elemental analysis was
48
49
50
51
52
53
54
55
56
57
58
59
60

1
2
3 performed with an inductively coupled plasma-mass spectrometry (ICP-MS) (PerkinElmer
4 NexION 300D equipped with Elemental Scientific Inc. autosampler and Apex HF sample
5 introduction system; PerkinElmer LAS Ltd, Seer Green, UK and Elemental Scientific Inc.,
6 Omaha, NE, USA, respectively) in the standard mode. Twenty elements (Li, B, Na, Mg, P, S, K,
7 Ca, Mn, Fe, Co, Ni, Cu, Zn, As, Se, Rb, Sr, Mo, and Cd) were monitored. Separate liquid
8 reference materials composed of pooled samples of the digested tissues (shoot, root and seed)
9 were prepared before the beginning of sample runs and were used throughout the samples runs.
10 They were run after every ninth sample in all ICP-MS sample sets, respectively, to correct for
11 variation between and within ICP-MS analysis runs⁵⁷. Sample concentrations were calculated
12 using external calibration method within the instrument software. The calibration standards (with
13 indium internal standard and blanks) were prepared from single element standards (Inorganic
14 Ventures; Essex Scientific Laboratory Supplies Ltd, Essex, UK) solutions.
15
16
17
18
19
20
21
22
23
24
25

26 **Synchrotron X-Ray Fluorescence**

27
28 Two-dimensional SXRF analysis was performed at various X-ray microprobe beamlines:
29 X26A (leaves in Figure 2B, Figure 3, and Supplemental Figure 4) and X27A (dry seeds in Figure
30 2E) of National Synchrotron Light Source (NSLS), Beamline 2-3 of Stanford Synchrotron
31 Radiation Lightsource (SSRL) (roots, leaves, and siliques of Figure 3B-D), XFM of the
32 Australian Synchrotron, (dry seeds in Figure 4F), and beamline 2-ID-D of the Advanced Photon
33 Source (APS) (Leaf tissue sections of Figure 4E). More details and metadata are found in the
34 Supplemental Methods.
35
36
37
38
39
40
41

42 **Real-time quantitative PCR**

43
44 RNA was prepared from plants grown on B5 medium for 2 weeks before transfer to +Fe
45 or -Fe media for 3 days. RNA extraction was performed using TRIzol® (Life Technologies) and
46 the RNEasy mini kit and protocol (Qiagen). Quantitative real-time PCR was performed on Step
47 One Plus Real Time PCR System (Applied Biosystems Version 2.2.3) using SYBR Premix
48 ExTaq reagents and protocol (Takara). Each sample was run in triplicate. Relative transcript
49 levels were calculated by normalizing to *EF1a* housekeeping expression.
50
51
52
53
54
55

56 **Microarray analysis**

1
2
3 RNA was extracted from three biological replicates as described above from root tissue
4 from plants grown on B5 medium for two weeks before transfer to either +Fe or –Fe medium for
5 3 days. RNA was labeled and hybridized to the Arabidopsis Gene 1.0 ST Arrays (Affymetrix) by
6 the Dartmouth Genomics and Microarray Laboratory. Raw data was RMA normalized using
7 Affymetrix Expression Console software and downstream analyses were performed using BRB-
8 Array Tools Version 4.2.1. BRB-ArrayTools is an integrated software package for the analysis of
9 DNA microarray data which was developed by the Biometric Research Branch of the Division of
10 Cancer Treatment & Diagnosis of the National Cancer Institute under the direction of Dr.
11 Richard Simon. Differentially expressed genes were identified between two classes using a
12 random-variance t-test with a p-value cutoff of 0.01. The random-variance t-test is an
13 improvement over the standard separate t-test as it permits sharing information among genes
14 about within-class variation without assuming that all genes have the same variance⁵⁸. We also
15 used a cutoff of 1.5 fold change up or down in response to Fe treatment for either wild type or
16 *bts-3*. Biological replicates for root and shoot arrays were averaged for analysis of gene
17 expression in each tissue. Hierarchical clustering was employed to generate heat maps for
18 subsets of significant genes using the open source software Cluster/Treeview^{59, 60}. GO term
19 enrichment using the DAVID Go Ontology program Functional Annotation Clustering tool using
20 an enrichment cutoff of >1.3 as previously described^{42, 43}. Microarray data was made publically
21 available in the GEO repository (<http://www.ncbi.nlm.nih.gov/geo>).
22
23
24
25
26
27
28
29
30
31
32
33
34
35
36
37
38

39 **Ferric chelate reductase assay**

40 Plants were grown for 2 weeks on B5 medium and then transferred to either +Fe or –Fe
41 media for 3 days. 5 plants were pooled for root Fe(III)-chelate reductase activity measurements,
42 as previously described⁵⁴.
43
44
45
46
47
48

49 **Protein isolation and immunodetection**

50 Wild type and *bts-3* plants were grown for 2 weeks on B5 medium and transferred to +Fe
51 or –Fe media for 3 days. Total protein was extracted from roots using protein extraction buffer:
52 50 mM Tris, pH8, 5% glycerol, 4%SDS, 1%PVPP, 2 mM Pefabloc (Roche), 1X Protease
53
54
55
56
57
58
59
60

1
2
3 Inhibitor Cocktail (Roche). SDS-PAGE followed by western electroblotting was performed and
4 blots were probed with an IRT1 antibody or α -tubulin antibody (AbCam).
5
6
7

8 **Accession Numbers**

9
10 Sequence data from this article can be found in the EMBL/GenBank data libraries under
11 accession numbers At3g18290 (*BTS*), At1g74770 (*BTSL1*), and At1g18910 (*BTSL2*).
12
13
14

15 **Acknowledgments**

16
17 We thank Brett Lahner and Elana Yakubov for performing the ICP-MS analysis and plant
18 growth and harvesting, respectively, for the screen of EMS mutagenized plants. In memoriam,
19 we thank John Danku for all the ICP-MS analyses included in this manuscript. Microarray
20 analysis was carried out at the Geisel School of Medicine in the Genomics Shared Resource,
21 which was established by equipment grants from the NIH and NSF and is supported in part by a
22 Cancer Center Core Grant (P30CA023108) from the National Cancer Institute. We thank
23 Amanda Socha for help with RNA extraction for microarray analysis and Carol Ringelberg for
24 her help with microarray data analysis. We thank Suzana Car for her help with SXRF
25 experiments at NSLS. We thank Sue Wirick and William Rao for their help at X26A and Ryan
26 Tappero for his help at X27A. X26A is supported by the Department of Energy (DOE) -
27 Geosciences (DE-FG02-92ER14244 to The University of Chicago - CARS). Use of the NSLS
28 was supported by DOE under Contract No. DE-AC02-98CH10886. X27A is supported in part by
29 the U.S. Department of Energy - Geosciences (DE-FG02-92ER14244 to The University of
30 Chicago - CARS) and Brookhaven National Laboratory– Department of Environmental
31 Sciences. Use of the NSLS was supported by the U.S. Department of Energy, Office of Science,
32 Office of Basic Energy Sciences, under Contract No. DE-AC02-98CH10886. We thank Sam
33 Webb and Benjamin Kocar for their help at Beamline 2-3 at SSRL. Use of the Stanford
34 Synchrotron Radiation Lightsource, SLAC National Accelerator Laboratory, is supported by the
35 U.S. Department of Energy, Office of Science, Office of Basic Energy Sciences under Contract
36 No. DE-AC02-76SF00515. The SSRL Structural Molecular Biology Program is supported by the
37 DOE Office of Biological and Environmental Research, and by the National Institutes of Health,
38 National Institute of General Medical Sciences (including P41GM103393). The contents of this
39 publication are solely the responsibility of the authors and do not necessarily represent the
40
41
42
43
44
45
46
47
48
49
50
51
52
53
54
55
56
57
58
59
60

1
2
3 official views of NIGMS or NIH. We thank Suna Kim and Louisa Howard for the help with
4 preparing leaf sections for Figure 4E. We thank Tony Lanzirrotti for his help at APS. Advanced
5 Photon Source, an Office of Science User Facility operated for the U.S. Department of Energy
6 (DOE) Office of Science by Argonne National Laboratory, was supported by the U.S. DOE
7 under Contract No. DE-AC02-06CH11357. We thank Martin DeJonge and Daryl Howard for
8 their help at XFM. This research was undertaken on the XFM beamline at the Australian
9 Synchrotron, Victoria, Australia. This work was supported by grants to M.L.G. from the US
10 National Science Foundation (DBI 0701119, IOS-0919941), the US National Institutes of
11 Health (R01GM078536), the US Department of Energy (DE-FG-2-06ER15809), and the US
12 National Institute of Environmental Health Sciences (P42 ES007373) and an NSF Plant Genome
13 grant (DBI 0701119) to D.E.S. and M.L.G. M.N.H. was supported by a National Science
14 Foundation Graduate Research Fellowship, a Nell Mondy Fellowship from Sigma Delta Epsilon-
15 Graduate Women in Science, and a Dartmouth Graduate Alumni Research Award.
16
17
18
19
20
21
22
23
24
25
26
27

28 **Figure legends**

29 **Figure 1. BTS, BTSL1, and BTSL2 are a family of closely-related RING E3 ligases**

30 **regulated by Fe deficiency.** A. BTS, BTSL1 and BTSL2 have very similar protein domain
31 architectures including hemerythrin domains and a C-terminal RING E3 ligase domain. The
32 RING domain is highly conserved among family members. Conserved Cys and His Zn²⁺-binding
33 residues for each C3H2C3 type RING are shown in red. The BTS Pro residue shown in blue is
34 mutated to Leu in *bts-3* plants. Protein domain structure was predicted by NCBI's conserved
35 domain database²⁹.
36

37 B. qPCR of *BTS*, *BTSL1* and *BTSL2* expression in roots and shoots of plants grown for 2 weeks
38 on B5 medium and then transferred to +Fe or -Fe medium for 3 days. Expression is relative to
39 EF1 α . Error bars represent SE (n=3).
40
41
42
43
44
45
46
47
48
49
50

51 **Figure 2. *bts* and *bts11/2* mutants have increased Fe concentrations and tolerance to Fe**

52 **deficiency.**
53 A. Chlorophyll levels were measured on plants grown for 10 days on B5 and then transferred to
54 -Fe medium for 7 days (n=3). Representative images of plants shown below. B. Representative
55
56
57
58
59
60

1
2
3
4
5
6
7
8
9
10
11
12
13
14
15
16
17
18
19
20
21
22
23
24
25
26
27
28
29
30
31
32
33
34
35
36
37
38
39
40
41
42
43
44
45
46
47
48
49
50
51
52
53
54
55
56
57
58
59
60

SXRF scans showing Fe localization in leaf #5 of plants grown for 2 weeks on B5 and then transferred to +Fe medium for 3 days. **C.** Root and shoot ICP-MS measurements of plants grown for 2 weeks on B5 and then transferred to +Fe or –Fe medium for 3 days (n=3) **D.** Seed ICP-MS measurements from soil grown plants (n=5). **E.** Representative SXRF scan showing Fe localization in mature, dry seed. In panels A, C, and D, lower case letters indicate significant differences at $p < 0.05$ (ANOVA with Tukey's). Error bars indicate SE.

Figure 3. *bts* and *bts11/2* mutants store more Fe, Zn and Mn in veins, hydathodes and trichomes than wild type.

SXRF scans showing Fe, Zn, and Mn localization in leaf #5 of plants grown for 2 weeks on B5 medium and then transferred to –Fe medium for 3 days.

Figure 4. *bts-3* has high concentrations of Fe in roots, leaves, and seeds.

A. ICP-MS measurements of roots and shoots of plants grown for 2 weeks on B5 medium and then transferred to +Fe or –Fe medium for 3 days (n=3). ICP-MS measurements of seeds from soil-grown plants (n=5 plants). * $p < 0.05$ between genotypes (student's t-test). Error bars indicate SE. **B.** Representative SXRF scans of root tips of plants grown for 7 days on B5 medium and then transferred to –Fe medium for 3 days. **C.** SXRF scan of leaf #8 showing Fe in red. **D.** SXRF scan showing Fe (red), Zn (green), Mn (blue) localization in developed, green siliques. **E.** SXRF scan showing Fe localization in resin-embedded shoot primary vein cross sections. Plants were grown on B5 medium for 2 weeks. Bright field light microscopy images of adjacent sections stained with toluidine blue are shown for reference. X indicates xylem and P indicates phloem **F.** SXRF images show Fe localization to the vasculature in individual seeds.

Figure 5. *bts-3* is tolerant to Fe-deficient growth conditions, but sensitive to Fe sufficient conditions and this phenotype can be complemented by *BTS* expression.

A. Plants were grown for 2 weeks on normal, alkaline, and alkaline +Fe soil. **B.** Plants were grown vertically for 5 days on B5 medium and then transferred to +Fe or –Fe medium for 7 days. **C.** SXRF scans showing Fe localization in leaf #5 of plants grown for 2 weeks on B5 medium and then transferred to +Fe medium for 3 days. *ProBTS:BTS bts-3* is the complementation line

1
2
3 where the *BTS* gene driven by its own promoter is expressed in the *bts-3* mutant. **D.** Plants were
4 grown vertically for 5 days on B5 medium and then transferred to +Fe or –Fe medium for 7 days.
5
6
7

8
9 **Figure 6. The Strategy I Fe deficiency response is on under +Fe conditions in *bts-3*.**

10 A. qPCR of *FRO2* and *IRT1* expression in roots of plants grown for 2 weeks on B5 medium and
11 then transferred to +Fe or –Fe medium for 3 days. Expression is relative to *EF1 α* . Error bars
12 represent SE (n=3).
13
14

15 B. Root ferric chelate reductase assay of plants grown for 2 weeks on B5 medium before transfer
16 to +Fe or –Fe medium for 3 days. *p<0.05 comparison between genotypes on +Fe conditions
17 (Student's t-test). Error bars indicate SE (n=3).
18
19

20 C. Representative *IRT1* western blot of roots of plants as grown in panel A. α -tubulin was used
21 as a loading control.
22
23
24
25

26
27 **Figure 7. Heat map of genes regulated by Fe in roots of wild type and *bts-3* plants.**

28 Microarray analysis of plants grown for 2 weeks on B5 medium and then transferred to +Fe or –
29 Fe medium for 3 days. Hierarchical clustering analysis was performed on genes which were 1.5
30 fold up or down regulated in response to Fe treatment in either genotype. Subsets 1-4 are
31 numbered and enriched GO terms (right) and known metal homeostasis genes (left) are shown.
32
33 The heat map was made with Java TreeView and GO terms predicted by DAVID 6.7^{42, 43, 60}.
34
35
36
37
38

39 **Figure 8. Model of BTS activity in roots of wild type vs. *bts-3*.**

40 In wild type, Fe binding via HHE domains may stabilize BTS protein, allowing for assembly of
41 E3 ligase machinery and subsequent target degradation. If the target is a positive regulator of the
42 Fe deficiency response, the Fe deficiency response is turned off. In –Fe conditions, lack of Fe
43 binding to HHE domains may lead to BTS protein degradation and accumulation and action of
44 positive regulators of the Fe deficiency response. In *bts-3*, if the mutation prevents interaction
45 with E2 enzymes, BTS protein cannot act as an E3 ligase, regardless of Fe status. In this case, its
46 target would always be able to induce the Fe deficiency response.
47
48
49
50
51
52

53 **Supplemental Data**

54 **Supplemental Figure 1.** Location of T-DNA insertions of *bts-1*, *bts11* and *bts12* mutants.
55
56
57
58
59
60

Supplemental Figure 2. *bts-1*, *bts11 bts12*, *bts-1 bts11 bts12*, and *bts-3* mutants all exhibit tolerance to Fe-deficient growth conditions, but only *bts-3* is sensitive to Fe-sufficient conditions.

Supplemental Figure 3. BTS family E3 ligase mutants have higher Mn and Zn concentrations in roots, shoots and seeds compared to wild type.

Supplemental Figure 4. Expression of *BTS* controlled by its endogenous promoter in *bts-3* returns Mn and Zn levels to wild type levels.

Supplemental Figure 5. Unlike *bts-3*, *bts-1 bts11 bts12* mutants do not exhibit induction of ferric chelate reductase activity when grown under Fe-sufficient conditions.

Supplemental Figure 6. *bts-3* roots exhibit constitutive expression of Fe deficiency genes.

Supplemental Methods. SXRF analysis.

References

1. M. N. Hindt and M. L. Guerinot, Getting a sense for signals: Regulation of the plant iron deficiency response, *BBA Mol. Cell. Res.*, 2012, **1823**, 1521-1530.
2. S. Santi and W. Schmidt, Dissecting iron deficiency-induced proton extrusion in Arabidopsis roots, *New Phytol.*, 2009, **183**, 1072-1084.
3. N. J. Robinson, C. M. Procter, E. L. Connolly and M. L. Guerinot, A ferric-chelate reductase for iron uptake from soils, *Nature*, 1999, **397**, 694-697.
4. J. Rodriguez-Celma, W. D. Lin, G. M. Fu, J. Abadia, A. Lopez-Millan and W. Schmidt, Mutually exclusive alterations in secondary metabolism are critical for uptake of insoluble iron compounds by Arabidopsis and *Medicago truncatula*, *Plant Physiol.*, 2013, **162**, 1473-1485.
5. N. B. Schmid, R. F. Giehl, S. Doll, H. P. Mock, N. Strehmel, D. Scheel, X. Kong, R. C. Hider and N. von Wiren, Feruloyl-CoA 6'-Hydroxylase1-dependent coumarins mediate iron acquisition from alkaline substrates in Arabidopsis, *Plant Physiol.*, 2014, **164**, 160-172.
6. H. Schmidt, C. Günther, M. Weber, C. Spörlein, S. Loscher, C. Böttcher, R. Schobert and S. Clemens, Metabolome analysis of *Arabidopsis thaliana* roots identifies a key metabolic pathway for iron acquisition, *PLoS ONE*, 2014, **9**, e102444.

- 1
2
3 7. P. Fourcroy, P. Siso-Terraza, D. Sudre, M. Saviron, G. Reyt, F. Gaymard, A. Abadia, J.
4 Abadia, A. Alvarez-Fernandez and J. F. Briat, Involvement of the ABCG37 transporter in
5 secretion of scopoletin and derivatives by Arabidopsis roots in response to iron
6 deficiency, *New Phytol.*, 2014, **201**, 155-167.
- 7
8
9
10 8. D. Eide, M. Broderius, J. Fett and M. L. Guerinot, A novel iron-regulated metal
11 transporter from plants identified by functional expression in yeast, *Proc. Natl. Acad. Sci.*
12 *U.S.A.*, 1996, **93**, 5624-5628.
- 13
14
15 9. G. Vert, N. Grotz, F. Dedaldechamp, F. Gaymard, M. L. Guerinot, J.-F. Briat and C.
16 Curie, IRT1, an Arabidopsis transporter essential for iron uptake from the soil and plant
17 growth., *Plant Cell*, 2002, **14**, 1223-1233.
- 18
19
20
21 10. R. Henriques, J. Jásik, M. Klein, E. Martinoia, U. Feller, J. Schell, M. S. Pais and C.
22 Koncz, Knock-out of Arabidopsis metal transporter gene *IRT1* results in iron deficiency
23 accompanied by cell differentiation defects, *Plant Mol. Biol.*, 2002, **50**, 587-597.
- 24
25
26 11. C. Varotto, D. Maiwald, P. Pesaresi, P. Jahns, S. Francesco and D. Leister, The metal ion
27 transporter IRT1 is necessary for iron homeostasis and efficient photosynthesis in
28 *Arabidopsis thaliana*, *Plant J.*, 2002, **31**, 589-599.
- 29
30
31 12. E. P. Colangelo and M. L. Guerinot, The essential bHLH protein FIT1 is required for the
32 iron deficiency response, *Plant Cell*, 2004, **16**, 3400-3412.
- 33
34
35 13. M. Jakoby, H.-Y. Wang, W. Reidt, B. Weisssharr and P. Bauer, FRU(BHLH029) is
36 required for induction of iron mobilization genes in *Arabidopsis thaliana*, *FEBS Lett.*,
37 2004, **577**, 528-534.
- 38
39
40 14. Y. X. Yuan, J. Zhang, D. W. Wang and H. Q. Ling, AtbHLH29 of *Arabidopsis thaliana*
41 is a functional ortholog of tomato FER involved in controlling iron acquisition in strategy
42 I plants, *Cell Res.*, 2005, **15**, 613-621.
- 43
44
45 15. H.-Y. Wang, M. Klatte, M. Jacoby, H. Baumlein, B. Weisshaar and P. Bauer, Iron
46 deficiency-mediated stress regulation of four subgroup Ib bHLH genes in *Arabidopsis*
47 *thaliana*, *Planta*, 2007, **226**, 897-908.
- 48
49
50 16. Y. Yuan, H. Wu, N. Wang, J. KLi, W. Zhao, J. Du, D. Wang and H.-Q. Ling, FIT
51 interacts with AtbHLH38 and AtbHLH39 in regulating iron uptake gene expression for
52 iron homeostasis in Arabidopsis, *Cell Res.*, 2008, **18**, 385-397.
- 53
54
55
56
57
58
59
60

17. N. Wang, Y. Cui, Y. Liu, H. Fan, J. Du, Z. Huang, Y. Yuan, H. Wu and H. Q. Ling, Requirement and functional redundancy of Ib subgroup bHLH proteins for iron deficiency responses and uptake in *Arabidopsis thaliana*, *Mol. Plant*, 2013, **6**, 503-513.
18. C. M. Palmer, M. N. Hindt, H. Schmidt, S. Clemens and M. L. Guerinot, MYB10 and MYB72 are required for growth under iron-limiting conditions, *Plos Genet.*, 2013, **9**, e1003953.
19. C. Zamioudis, J. Hanson and C. M. Pieterse, β -Glucosidase BGLU42 is a MYB72-dependent key regulator of rhizobacteria-induced systemic resistance and modulates iron deficiency responses in *Arabidopsis* roots, *New Phytol.*, 2014, **204**, 368-379.
20. T. A. Long, H. Tsukagoshi, W. Busch, B. Lahner, D. E. Salt and P. N. Benfey, The bHLH transcription factor POPEYE regulates response to iron deficiency in *Arabidopsis* roots, *Plant Cell*, 2010, **22**, 2219-2236.
21. R. A. Rampey, A. W. Woodward, B. N. Hobbs, M. P. Tierney, B. Lahner, D. E. Salt and B. Bartel, An *Arabidopsis* basic helix-loop-helix leucine zipper protein modulates metal homeostasis and auxin conjugate responsiveness, *Genetics*, 2006, **174**, 1841-1857.
22. J. Zhang, B. Liu, M. Li, D. Feng, H. Jin, P. Wang, J. Liu, F. Xiong, J. Wang and H.-B. Wang, The bHLH Transcription Factor bHLH104 Interacts with IAA-LEUCINE RESISTANT3 and Modulates Iron Homeostasis in *Arabidopsis*, *Plant Cell*, 2015, **3**, 787-805.
23. D. Selote, R. Samira, A. Matthiadis, J. W. Gillikin and T. A. Long, Iron-binding E3 ligase mediates iron response in plants by targeting basic helix-loop-helix transcription factors, *Plant Physiol.*, 2015, **167**, 273-286.
24. X. Li, H. Zhang, Q. Ai, G. Liang and D. Yu, Two bHLH transcription factors, bHLH34 and bHLH104, regulate iron homeostasis in *Arabidopsis thaliana*, *Plant Physiol.*, 2016, **170**, 2478-2493.
25. A. Matthiadis and T. A. Long, Further insight into BRUTUS domain composition and functionality, *Plant Signal. Behav.*, 2016, **11**, e1204508.
26. J. McElver, I. Tzafirir, G. Aux, R. Rogers, C. Ashby, K. Smith, C. Thomas, A. Schetter, Q. Zhou and M. A. Cushman, Insertional mutagenesis of genes required for seed development in *Arabidopsis thaliana*, *Genetics*, 2001, **159**, 1751-1763.

- 1
2
3
4
5
6
7
8
9
10
11
12
13
14
15
16
17
18
19
20
21
22
23
24
25
26
27
28
29
30
31
32
33
34
35
36
37
38
39
40
41
42
43
44
45
46
47
48
49
50
51
52
53
54
55
56
57
58
59
60
27. P. Kersey, J. Allen, M. Christensen, P. Davis, L. Falin, C. Grabmueller, D. Hughes, J. Humphrey, A. Kerhornou and J. Khobova, *Ensembl Genomes 2013: scaling up access to genome-wide data*, *Nucleic Acids Res.*, 2014, **42**, 546-552.
 28. M. A. Larkin, G. Blackshields, N. P. Brown, R. Chenna, P. A. McGettigan, H. McWilliam, F. Valentin, I. M. Wallace, A. Wilm, R. Lopez, J. D. Thompson, T. J. Gibson and D. G. Higgins, *Clustal W and Clustal X version 2.0*, *Bioinformatics*, 2007, **23**, 2947-2948.
 29. A. Marchler-Bauer, M. K. Derbyshire, N. R. Gonzales, S. Lu, F. Chitsaz, L. Y. Geer, R. C. Geer, J. He, M. Gwadz, D. I. Hurwitz, C. J. Lanczycki, F. Lu, G. H. Marchler, J. S. Song, N. Thanki, Z. Wang, R. A. Yamashita, D. Zhang, C. Zheng and S. H. Bryant, *CDD: NCBI's conserved domain database*, *Nucleic Acids Res.*, 2015, **43**, D222-226.
 30. T. Kobayashi, S. Nagasaka, T. Senoura, R. N. Itai, H. Nakanishi and N. K. Nishizawa, *Iron-binding haemerythrin RING ubiquitin ligases regulate plant iron responses and accumulation*, *Nat. Commun.*, 2013, **4**, 2792.
 31. S. A. Kim, T. Punshon, A. Lanzirotti, L. Li, J. M. Alonso, J. R. Ecker, J. Kaplan and M. L. Guerinot, *Localization of iron in Arabidopsis seed requires the vacuolar membrane transporter VIT1*, *Science*, 2006, **314**, 1295-1298.
 32. Y. O. Korshunova, D. Eide, W. G. Clark, M. L. Guerinot and H. B. Pakrasi, *The IRT1 protein from Arabidopsis thaliana is a metal transporter with a broad substrate range*, *Plant Mol. Biol.*, 1999, **40**, 37-44.
 33. B. Lahner, J. Gong, M. Mahmoudian, E. L. Smith, K. B. Abid, E. E. Rogers, M. L. Guerinot, J. F. Harper, J. M. Ward, L. McIntyre, J. I. Schroeder and D. E. Salt, *Genomic scale profiling of nutrient and trace elements in Arabidopsis thaliana*, *Nat. Biotechnol.*, 2003, **21**, 1215-1221.
 34. I. Baxter, P. S. Hosmani, A. Rus, B. Lahner, J. O. Borevitz, B. Muthukumar, M. V. Mickelbart, L. Schreiber, R. B. Franke and D. E. Salt, *Root suberin forms an extracellular barrier that affects water relations and mineral nutrition in Arabidopsis*, *PLoS Genet.*, 2009, **5**, e1000492. .
 35. H. Tian, I. R. Baxter, B. Lahner, A. Reinders, D. E. Salt and J. M. Ward, *Arabidopsis NPCC6/NaKR1 is a phloem mobile metal binding protein necessary for phloem function and root meristem maintenance*, *Plant Cell*, 2010, **22**, 3963-3979.

- 1
2
3
4
5
6
7
8
9
10
11
12
13
14
15
16
17
18
19
20
21
22
23
24
25
26
27
28
29
30
31
32
33
34
35
36
37
38
39
40
41
42
43
44
45
46
47
48
49
50
51
52
53
54
55
56
57
58
59
60
36. D.-Y. Chao, K. Gable, M. Chen, I. Baxter, C. R. Dietrich, E. B. Cahoon, M. L. Guerinot, B. Lahner, S. Lu, J. E. Markham, J. Morrissey, J. Han, S. D. S.D. Gupta, J. M. Harmon, J. G. Jaworski, T. M. Dunn and D. E. Salt., Sphingolipids in the root play an important role in regulating the leaf ionome in *Arabidopsis thaliana*, *Plant Cell*, 2011, **23**, 1061-1081.
 37. M. Borghi, A. Rus and D. E. Salt, Loss-of-function of constitutive expresser of Pathogenesis Related Genes5 affects potassium homeostasis in *Arabidopsis thaliana*, *PLoS One*, 2011, **6**, e26360.
 38. T. Kamiya, M. Borghi, P. Wang, J. M. Danku, L. Kalmbach, P. S. Hosmani, S. Naseer, T. Fujiwara, N. Geldner and D. E. Salt, The MYB36 transcription factor orchestrates Casparian strip formation, *Proc. Natl. Sci. U.S.A.*, 2015, **112**, 10533-10538.
 39. A. Becker, D. Y. Chao, X. Zhang, D. E. Salt and I. Baxter, Bulk segregant analysis using single nucleotide polymorphism microarrays, *PLoS One*, 2011, **6**, e15993.
 40. D. Y. Chao, A. Silva, I. Baxter, Y. S. Huang, M. Nordborg, J. Danku, B. Lahner, E. Yakubova and D. E. Salt, Genome-wide association studies identify Heavy Metal ATPase3 as the primary determinant of natural variation in leaf cadmium in *Arabidopsis thaliana*, *PLoS Genet.*, 2012, **8**, e1002923.
 41. D. Y. Chao, Y. Chen, J. Chen, S. Shi, Z. Chen, C. Wang, J. M. Danku, F. J. Zhao and D. E. Salt, Genome-wide association mapping identifies a new arsenate reductase enzyme critical for limiting arsenic accumulation in plants, *PLoS Biol.*, 2014, **12**, e1002009.
 42. D. W. Huang, B. T. Sherman and R. A. Lempicki, Systematic and integrative analysis of large gene lists using DAVID bioinformatics resources, *Nat. Protoc.*, 2009, **4**, 44-57.
 43. D. W. Huang, B. T. Sherman and R. A. Lempicki, Bioinformatics enrichment tools: paths toward the comprehensive functional analysis of large gene lists, *Nucleic Acids Res.*, 2009, **37**, 1-13.
 44. A. A. Salahudeen, J. W. Thompson, J. C. Ruiz, H. W. Ma, L. N. Kinch, Q. Li, N. V. Grishin and R. K. Bruick, An E3 ligase possessing an iron-responsive hemerythrin domain is a regulator of iron homeostasis, *Science*, 2009, **326**, 722-726.
 45. A. A. Vashisht, K. B. Zumbrennen, X. Huang, D. N. Powers, A. Durazo, D. Sun, N. Bhaskaran, A. Persson, M. Uhlen, O. Sangfelt, C. Spruck, E. A. Leibold and J. A. Wohlschlegel, Control of iron homeostasis by an iron-regulated ubiquitin ligase, *Science*, 2009, **326**, 718-721.

- 1
2
3 46. R. J. Deshaies and C. A. Joazeiro, RING domain E3 ubiquitin ligases, *Annu. Rev.*
4 *Biochem.*, 2009, **78**, 399-434.
5
6
7 47. N. Zheng, P. Wang, P. D. Jeffrey and N. P. Pavletich, Structure of a c-Cbl-UbcH7
8 Complex: RING domain function in ubiquitin-protein ligases, *Cell*, 2000, **102**, 533-539.
9
10 48. P. D. Mace, K. Linke, R. Feltham, F. R. Schumacher, C. A. Smith, D. L. Vaux, J. Silke
11 and C. L. Day, Structures of the cIAP2 RING domain reveal conformational changes
12 associated with ubiquitin-conjugating enzyme (E2) recruitment, *J. Biol. Chem.*, 2008,
13 **283**, 31633-31640.
14
15
16 49. Q. Yin, B. Lamothe, B. G. Darnay and H. Wu, Structural basis for the lack of E2
17 interaction in the RING domain of TRAF2, *Biochemistry*, 2009, **48**, 10558-10567.
18
19 50. Q. Yin, S. C. Lin, B. Lamothe, M. Lu, Y. C. Lo, G. Hura, L. Zheng, R. L. Rich, A. D.
20 Campos, D. G. Myszka, M. J. Lenardo, B. G. Darnay and H. Wu, E2 interaction and
21 dimerization in the crystal structure of TRAF6, *Nat. Struct. Mol. Biol.*, 2009, **16**, 658-
22 666.
23
24
25 51. D. E. Spratt, R. Julio Martinez-Torres, Y. J. Noh, P. Mercier, N. Manczyk, K. R. Barber,
26 J. D. Aguirre, L. Burchell, A. Purkiss, H. Walden and G. S. Shaw, A molecular
27 explanation for the recessive nature of parkin-linked Parkinson's disease, *Nat. Commun.*,
28 2013, **4**, 1983.
29
30 52. A. Sivitz, C. Grinvalds, M. Barberon, C. Curie and G. Vert, Proteasome-mediated
31 turnover of the transcriptional activator FIT is required for plant iron-deficiency
32 responses, *Plant J.*, 2011, **66**, 1044-1052.
33
34 53. H. Marschner, V. Römheld and H. Ossenberg-Neuhaus, Rapid method for measuring
35 changes in pH and reducing processes along roots of intact plants, *Z. Pflanzenphysiol.* ,
36 1982, **105**, 407-416.
37
38 54. Y. Yi and M. L. Guerinot, Genetic evidence that induction of root Fe(III) chelate
39 reductase activity is necessary for iron uptake under iron deficiency, *Plant J.*, 1996, **10**,
40 835-844.
41
42 55. S. J. Clough and A. F. Bent, Floral dip: a simplified method for *Agrobacterium*-mediated
43 transformation of *Arabidopsis thaliana*, *Plant J.*, 1998, **16**, 735-743.
44
45 56. L. Harmutk, Chlorophylls and carotenoids: Pigments of photosynthetic biomembranes,
46 *Methods Enzymol.*, 1987, **34**, 350-382.
47
48
49
50
51
52
53
54
55
56
57
58
59
60

- 1
2
3
4
5
6
7
8
9
10
11
12
13
14
15
16
17
18
19
20
21
22
23
24
25
26
27
28
29
30
31
32
33
34
35
36
37
38
39
40
41
42
43
44
45
46
47
48
49
50
51
52
53
54
55
56
57
58
59
60
57. J. C. Danku, B. Lahner, E. Yakubova and D. Salt, in *Plant Min. Nutr.*, ed. F. J. M. Maathuis, Humana Press, 2013, vol. 953, ch. 17, pp. 255-276.
 58. G. W. Wright and R. M. Simon, A random variance model for detection of differential gene expression in small microarray experiments, *Bioinformatics*, 2003, **19**, 2448-2455.
 59. M. B. Eisen, P. T. Spellman, P. O. Brown and D. Botstein, Cluster analysis and display of genome-wide expression patterns, *Proc. Natl. Acad. Sci. USA.*, 1998, **95**, 14863-14868.
 60. A. J. Saldanha, Java Treeview--extensible visualization of microarray data, *Bioinformatics*, 2004, **20**, 3246-3248.